How Do Liquid Mixtures Solubilize Insoluble Gelators? Self-Assembly Properties of Pyrenyl-Linker-Glucono Gelators in Tetrahydrofuran–Water Mixtures

Ni Yan,[†,‡] Zhiyan Xu,[†] Kevin K. Diehn,[§] Srinivasa R. Raghavan,[§] Yu Fang,*[,†] and Richard G. Weiss*[,‡,∥]

[†]Key Laboratory of Applied Surface and Colloid Chemistry (Ministry of Education), School of Chemistry and Chemical Engineering, Shaanxi Normal University, Xi'an 710062, P. R. China

[‡]Department of Chemistry and [∥]Institute for Soft Matter Synthesis and Metrology, Georgetown University, Washington, D.C. 20057-1227, United States

[§]Department of Chemical and Biomolecular Engineering, University of Maryland, College Park, Maryland 20742-2111, United States

S *Supporting Information*
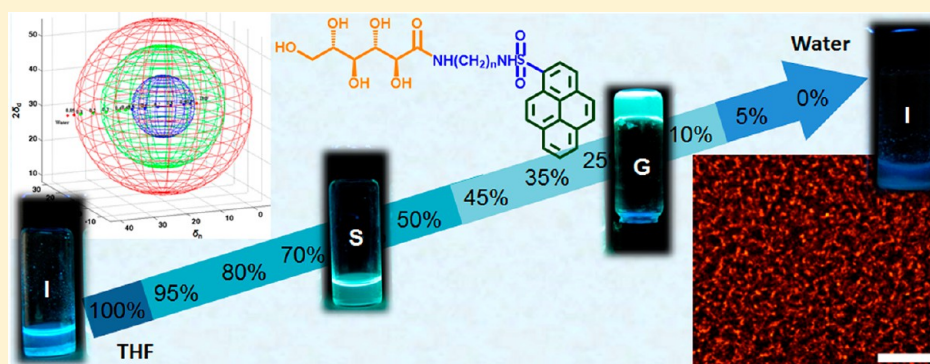
ABSTRACT: The self-assembly behavior of a series of glucono-appended 1-pyrenesulfonyl derivatives containing α,ω-diaminoalkane spacers (**P**n, where n, the number of methylene units separating the amino groups, is 2, 3, 4, 6, 7, and 8) in v:v tetrahydrofuran (THF):water mixtures is examined at room temperature. The **P**n at 2 w/v % concentrations do not dissolve in either THF or water at room temperature. However, the **P**n can be dissolved in some THF:water mixtures, and they form gels spontaneously in other compositions without dissolving completely. The self-assembly of the **P**n in the liquid mixtures has been investigated using a variety of techniques. The particle sizes of the **P**n in their solutions/sols, critical gelation concentrations, microstructures, thermal and mechanical stabilities of the gels, and molecular packing modes of **P**n molecules in their gel networks are found to be very dependent on the composition of the liquid mixtures. Correlations between the self-assembly behavior of the **P**n and the polarity of the liquid mixtures, as probed by $E_T(30)$ and Hansen solubility parameters, yield both qualitative and quantitative insights into why self-assembly of the **P**n can or cannot be achieved in different liquid compositions. As revealed by UV–vis and fluorescence spectroscopy studies, π–π stacking of the pyrenyl groups occurs as part of the aggregation process. Correlations between the rheological properties of the gels and the Hansen solubility parameters of the **P**n and the solvent mixtures indicate that hydrogen-bonding interactions are a major contributor to the mechanical stability. Overall, the results of this study offer a new strategy to investigate the balance between dissolution and aggregation of molecular gelators. To the best of our knowledge, this is the first example of the spontaneous formation of molecular gels without heating by placing gelators in mixtures of liquids in which they are insoluble in the neat components.

■ INTRODUCTION

The gelation phenomenon exhibited by low molecular mass gelators (LMMGs) has received increasing attention because of the growing number of applications of gels[1−3] and their role in learning how to control one-dimensional self-assembly.[4−6] LMMGs can self-assemble into fibers, rods, ribbons, or other aggregates of different morphologies in suitable liquids through hydrogen bonding, π–π stacking, London dispersion forces, and other types of van der Waals interactions, leading to the formation of three-dimensional networks which are needed to

form a gel.[4] The weakness of these interactions,[7] compared with covalent bonds, makes these gels intrinsically more likely to be stimulus-responsive than polymer-based gels. Stimuli including heat, light,[8] ultrasound,[9] shearing stress,[10] pH,[11] host–guest interactions,[12] metallic ions,[13] and oxidative/reductive reactions[14] have been demonstrated to affect the sol–gel transitions of LMMG-liquid mixtures.

The gelation process is controlled in part by the balance between the tendency of the gelator molecules to remain dissolved or to aggregate in a liquid.[15] Some amphiphilic compounds can gelate a wide range of liquids, including both water and organic solvents. In water, their hydrophobic groups promote aggregation and hydrophilic groups provide solubility; in organic liquids, aggregation is promoted by the hydrophilic groups and dissolution from hydrophobic groups. In our previous work, 2-naphthyl[16] or 1-pyrenyl[17] as a hydrophobic group and glucono as a hydrophilic moiety were separated by α,ω-diamine spacers of different lengths to yield fluorescent LMMGs. As a result of their ability to dissolve or aggregate in a particular neat liquid, the LMMGs containing shorter spacers were hydrogelators, those with somewhat longer spacers were ambidextrous, and the ones with the longest spacers were organogelators only.

Introducing a second gelator component can also affect the dissolution/aggregation balance. This strategy has been employed to promote gelation in several examples.[18−20] Another simple and versatile approach to effecting gelation is to introduce a second liquid component to one in which the LMMG could be well dissolved even without heating. The second component is usually miscible with the first and complements the first to promote aggregation and gelation.[21−27] Alternatively, the second component can be immiscible with the first, so that a two-phase gel-emulsion is formed in which one component is the dispersed phase and the other is the continuous phase.[28]

Previously, we found that glucono-appended 1-pyrenesulfonyl molecules containing α,ω-diaminoalkane spacers (**Pn**, Chart 1) cannot be dissolved in either THF or water at room

Chart 1. Molecular Structures of the Glucono-Pyrenyl Molecules (Pn, where n = 2, 3, 4, 6, 7, 8)
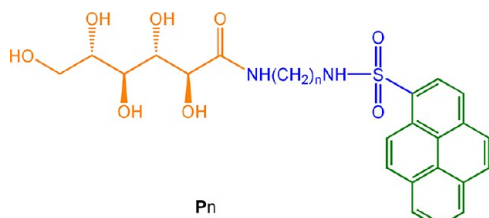
temperature.[17] Serendipitously, we found that, when poured together, **P7**/THF and **P7**/water solid–liquid mixtures became an opaque and stable gel after several seconds. To the best of our knowledge, this is the first example of two insoluble systems forming stable gels when mixed without heating or another perturbation. Subsequently, the influence of the composition of the miscible mixtures of THF and water[29] with 2 w/v % (hereafter referred to as %) **P7** on their aggregation was investigated: some formed solutions/sols in relatively high THF compositions; some formed gels in lower THF compositions; and some could not be dissolved in mixtures with high-water contents. In order to extend and gain a better understanding of the basis for this interesting phenomenon, we examine here: (1) the self-assembly behaviors of **Pn** in v:v THF:water mixtures; (2) the nature of the self-assembly behaviors of the **Pn** as a function of the composition of the THF–water mixtures; and (3) correlations between the $E_T(30)$ values of the mixtures and the Hansen solubility parameters (HSPs) of **Pn** and the mixtures. The insights derived from those results provide a new method to ascertain

the balance between dissolution and aggregation (i.e., how to promote gelation of specific liquids by new types of LMMGs).

EXPERIMENTAL SECTION

Materials. The **Pn** were prepared as described previously,[17] and the details are included in Supporting Information. The initially purified material, referred to as Series A, was used in all experiments except as noted in the text. In some experiments, Series A material was purified further to yield **Pn** denoted as Series B. 2,6-Diphenyl-4-(2,4,6-triphenylpyridiniophenolate) (Reichardt's dye, 95%, Aldrich) was used as received. Tetrahydrofuran (THF, reagent grade, > 99.0%, Sigma-Aldrich) was distilled before use. Water was deionized and distilled before use.

Gelation Tests. All **Pn** concentrations are expressed in % as the ratio of gelator weight (g) to liquid volume (mL). THF and water mixtures are expressed as volume ratios. A measured volume of water was added to a known weight of **Pn** and a measured volume of THF in a vial (1 × 4 cm). The mixture was shaken by hand for ∼30 s and then allowed to stand for 10 min. If no flow was detectable over a period of ∼10 s when the vial was inverted and there was no visual evidence of macroscopic phase separation, then the sample is designated as a gel (G). Systems with only liquid are referred to as solutions or sols (S). When a precipitate appeared after the gelator dissolved in a liquid or could not be dissolved, the designations are precipitate (P) and insoluble (I), respectively. Samples with microcrystalline **Pn** and which flowed when inverted are designated as suspensions (Sus). The I, P, and Sus systems were also heated at ∼60 °C in a water bath until the solid was dissolved. After the solutions/sols cooled to room temperature in air, the vials were inverted to determine whether the samples flowed perceptibly.

Two other methods to prepare samples for gelation tests were employed as well in selected cases. In one, a **Pn** was added directly to a THF:water mixture, which had been shown to be gelated using the method described above. After vortexing the mixture at ∼1000 rpm for ∼30 s and allowing it to stand for several hours, its appearance was noted. In the second, water was added to a **Pn** solution in 1:1 THF:water to effect different final compositions. As an example, 300 μL of THF and 300 μL of water were added to 20 mg of solid **P7**. The mixture became a transparent solution/sol after being shaken. After 400 μL of water was added (resulting in a 2% **P7** in 30:70 THF:water composition), the mixture was shaken for 30 s. Its appearance was noted after it had remained at rest for 10 min.

The reported critical gelator concentrations (CGCs) are the lowest **Pn** concentrations which produced gels when samples were prepared by the first method (i.e., at room temperature without heating or vortexing). Gelation temperatures (T_{gel}) are the ranges over which gels, inverted in flame-sealed tubes, fell under the influence of gravity when heated at ∼2 °C/min in a water bath.[30]

Calculation of HSPs. The overall energy density (δ) is separated into dispersive (δ_d), polar (δ_p), and hydrogen-bonding (δ_h) interaction components (eq 1):

$$\delta = \sqrt{{\delta_d}^2 + {\delta_p}^2 + {\delta_h}^2} \tag{1}$$

HSPs for THF and water were obtained from the literature.[31] THF is miscible with water at all compositions.[29] For their liquid mixtures, the solubility parameter (δ_i^{mix}) was taken as the sum of the products of the component solubility parameters and their volume fractions (φ), using eq 2:[32]

$$\delta_i^{mix} = \delta_i^{THF}\varphi_{THF} + \delta_i^{water}\varphi_{water} \tag{2}$$

Hansen space was calculated using UMD Complex Fluids and Nanomaterials Laboratory Hansen Solubility Parameter Data Fitting Software (version 1.3).[33] For the purpose of this analysis, the samples of the **Pn** in liquid mixtures were separated into soluble (S), gel (G), and insoluble (I) categories; suspensions and precipitates were treated as "insoluble". HSP values for each gelator were determined using data fitting of each Hansen space. The distances (R) between the gelator δ_p,

δ_h, and δ_d values and those of a liquid mixture (δ_p^{mix}, δ_h^{mix}, and δ_d^{mix}) in Hansen space were calculated using eq 3:

$$R = \sqrt{4(\delta_d - \delta_d^{mix})^2 + (\delta_p - \delta_p^{mix})^2 + (\delta_h - \delta_h^{mix})^2} \qquad (3)$$

Morphology Studies. Polarizing optical micrographs (POMs) were recorded on a Leitz 585 SM-LUX-POL microscope equipped with crossed polars, a Leitz 350 heating stage, a Photometrics CCD camera interfaced to a computer, and an Omega HH503 microprocessor thermometer connected to a J−K−T thermocouple. Samples were flame sealed in 0.4 or 0.5 mm path length, flattened pyrex capillary tubes (VitroCom). Scanning electron microscopy (SEM) images of s were taken on a Quanta 200 SEM spectrometer (Philips-FEI) at 20 kV and 10 mA. Solids from the solutions/sols of 2.0% **P7** in 95:5, 70:30, and 50:50 THF:water and xerogels from the gels of 2.0% **P7** in 40:60, 30:70, 25:75, and 20:80 mixtures were prepared by freeze-drying 1 mL of the solutions/sols or gels in a vial (1 × 4 cm) in an ALPHA1-2 freeze dryer (CHRIST) at −80 °C and ~4 Pa for 24 h. Prior to examination, the solid or xerogel was attached to a copper holder with conductive adhesive tape, and then it was sputter coated with a thin layer of gold using a SCD 005 cool sputter coater (Bal-Tec) at 30 mA and ~10 Pa for 80 s.

Dynamic Light Scattering (DLS) Measurements. Solutions/sols of **P7** were filtered and placed in 1 cm quartz cuvettes. A BI-90Plus Particle Size Analyzer (Brookhaven) operating at 660 nm was employed, and particle sizes were processed by 12CFR part II software.

Absorption Measurements. Absorption spectra were conducted on a Varian UV−visible (Cary 300 Bio) spectrophotometer at room temperature. Samples of **P7** in liquid mixtures were placed in 0.1 mm Hellma quartz cells (sealed with a Teflon cap). Samples of Reichardt's dye in liquid mixtures were placed in flattened pyrex capillary tubes (VitroCom) of 0.4 or 0.5 mm (0−10% water) or 4 or 5 mm path length (20−40% water), a 1 cm quartz cell (50−60% water), or a 7 cm quartz cell (70−100% water). The maximum absorbance wavelength (λ_{max}, nm) of Reichardt's dye in each liquid mixture was recorded. Transition energies ($E_T(30)$, kcal/mol) for the solvatochromic band of the dye in each liquid are calculated by means of eq 4:

$$E_T(30) = \hbar c N_A / \lambda_{max} = 28591 / \lambda_{max} \qquad (4)$$

where $\hbar$ is Planck's constant, c is the speed of the light in a vacuum, and N_A is Avogadro's number.[34]

Absorption spectra of the liquid phases from the two-phase mixtures of 0.15% or 2% **P7** in neat THF or in neat water and the spectra of the solutions of 8.7×10^{-5} M **P7** in neat THF or in neat water were recorded. The concentration of the liquid phase in neat THF was determined by comparing its absorbances at 280, 350, and 377 nm with the solution of 8.7×10^{-5} M **P7** in neat THF, calculated using Beer's law and averaged. The concentration of the liquid phase in neat water was determined using the same method but comparing the absorbances at 287, 360, and 379 nm. The concentrations of **Pn** in both THF and water were measured twice using new samples for each run and were averaged; the molar extinction coefficients were the same within experimental error in the two solvents.

Fluorescence. Emission spectra of the gel, solution/sol, and liquid phases from the two-phase mixtures of N$_2$-saturated 2% **P7** (Series B) in THF:water liquid mixtures in flame sealed 4 mm (width) × 7 mm (length) pyrex flattened capillaries (Vitro Dynamics, Inc.) were recorded in a front-face mode at an angle of ~45° with respect to the incident beam of a time-correlated single-photon-counting FLS 920 fluorescence spectrometer (Edinburgh) at 20 °C. The samples were prepared at room temperature without heating and cooling. In order to calculate the I_1/I_3 vibronic band intensity ratios of the monomeric component of the emission, the excimeric contributions to the monomeric emissions were subtracted using PeakFit V4.12 software (Systat Software, Inc.) and an empirical method in which the excimeric emission band was calculated by subtracting the emission spectrum of a N$_2$-saturated 1.1×10^{-5} M **P7** (Series B) in a THF:water mixture (normalized for intensity at the I_1 band) from a 3.5×10^{-2} M (2%) spectrum in the same THF:water composition. Then, the calculated

excimeric contribution was subtracted from the 3.5×10^{-2} M emission spectrum.

X-ray Diffraction (XRD) and Calculated Molecular Lengths. XRD diffractograms of neat powders, gels (of **P7** (Series B) and liquid mixtures were conducted on a Rigaku R-AXIS image plate system with Cu Kα X-rays (λ = 0.154 nm) generated by a Rigaku generator operating at 40 kV and 30 mA with the collimator at 0.5 mm. Data processing and analyses were conducted with Materials Data JADE (version 5.0.35) XRD pattern processing software. Samples were sealed in 1 mm (neat powder) or 0.5 mm (gel and liquid mixtures) glass capillaries (W. Müller, Schönwalde, Germany), and diffraction data were collected for 2 (neat powder) or 10 h (gel and liquid mixtures). The extended molecular lengths of the **Pn** were calculated using Materials Studio 4.3 software with the addition of the van der Waals radii[35] of terminal atoms.

Rheological Measurements. Measurements were performed using an Anton Paar Physica MCR 301 rheometer equipped with a Peltier temperature controller and parallel stainless steel plates (25 mm diameter, 0.5 mm gap). A liquid trap device was placed over the sample chamber to minimize evaporation. The data were collected using Rheoplus/32 Service V3.10 software. Before data were recorded, a hot aliquot of a **Pn** in a liquid was placed between the parallel plates of the rheometer and heated to 50 °C to ensure that a solution/sol was present. The sample was cooled to 5 °C at ~10 °C/min and incubated there for 10 min to reform the gel. Then, the temperature was increased to 25 °C and kept there for 8 min. Linear viscoelastic regions of the gel samples of 2% **P7** in liquid mixtures were determined by measuring the storage modulus, G' (associated with energy storage), and the loss modulus, G'' (associated with the loss of energy), as a function of the strain amplitude. Thereafter, the moduli were measured from 0.01 to 100 Hz at a constant shear strain in the linear region (0.1%). The strain sweeps of each **Pn** were measured 3 times and averaged using new samples for each run. Reported error limits are the difference between the value in one run and the average value.

NMR. ^{1}H and ^{13}C NMR spectra were recorded on Inova 400 MHz Spectrometer. Data processing and analyses were performed using Mercury software. Chemical shifts were referenced to an internal standard, tetramethylsilane (TMS).

Elemental Analyses. Elemental analyses were performed on a Perkin-Elmer 2400 CHN elemental analyzer using acetanilide as a calibration standard.

■ RESULTS AND DISCUSSION

Purification and Purity of the Pn. As noted previously,[17] the **Pn** are difficult to purify due to the presence of the glucono groups. The melting points of further purified **Pn** (Series B) were ~0.5 °C higher than those of the initially purified material (Series A), and their melting ranges are somewhat narrower (Table S1). In addition, elemental analyses of Series B **Pn** were closer to the values expected for a half-hydrate than those of Series A. Because the procedure for obtaining the Series B products is laborious and entails a significant loss of the product and the difference between the elemental analyses for the two series is relatively small, < 2%, we have used the Series A material except where greater purity was deemed necessary.

Gelation Properties. The **Pn** at 2% concentrations cannot be dissolved in neat THF or water at room temperature without heating.[17] However, the discovery that 2% of **P7** can form stable gels when the insoluble systems of **P7**/THF and **P7**/water are mixed at room temperature (Figure 1) has led us to examine in detail the gelation behavior of all of the **Pn** in different v:v THF:water compositions without heating, sonication, or other perturbations. All of the **Pn**, except **P2** and **P3**, could be solubilized well or transformed into gels at some THF:water compositions (Table 1).

The gelation results fall into two families of very similar behavior: **P2** and **P3** are one family and **P4−P8** are in another.
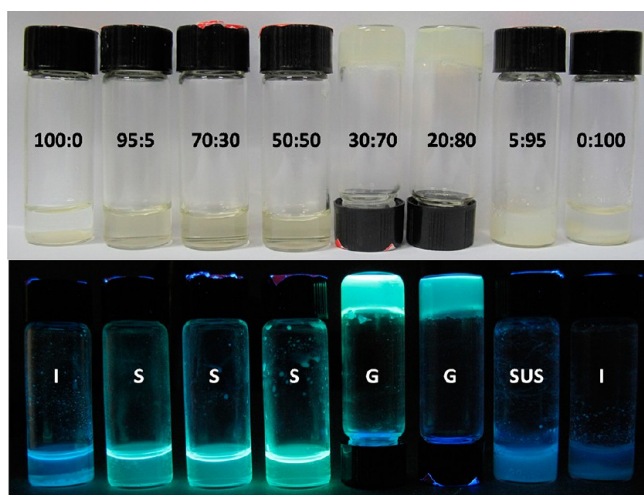
Figure 1. Pictures of 2% **P7** in THF:water mixtures at room temperature. Bottom: the same samples under a 365 nm irradiation.

Although **P2** and **P3** could not be dissolved in either neat THF or neat water at room temperature, they could be in mixtures of the two with 35−90% THF. Heating and then cooling samples with liquid compositions outside this range to room temperature or ~4 °C (for ~12 h) did not result in gels. **P4**−**P8** could not be dissolved in neat THF or water but were dissolved (clear, transparent solutions/sols) in mixtures with 5−50% water. **P4**−**P8** gelated liquid mixtures with ~55−90% water and yielded suspensions or remained insoluble in >90% water. Among **P4**−**P8**, **P7** gelated the broadest range of liquid compositions, and **P6** had the narrowest composition range. All of the samples which were suspensions or in which the **Pn** were

insoluble were dissolved at ~60 °C and cooled to room temperature to determine whether gelation could be induced thermally; the results were shown in Table 1. None produced a gel.

As expected, gels could be produced by vortexing samples vigorously (see Experimental Section) at room temperature. However, this process led to gels in only those cases where simple shaking by hand was effective; see, for example, results from 2% **P7** in 30:70 THF:water (Figure S1). The method in which water was added to a preformed solution/sol of **Pn** in 50:50 THF:water (see Experimental Section) also led to stable gels in those cases where the same **Pn** compositions and concentrations led to gels by shaking. Furthermore, based upon the similarity between the appearances and the T_{gel} values of the gels prepared using the three methods, their properties and structures are independent of the preparation procedure.

The CGCs of **Pn** (Table 1 and Figure S2) also changed with changing compositions of the liquid mixtures as expected. **P6** and **P7** are 'supergelators':[5] **P6** had very low CGC values, ~0.5%, throughout the composition range it gelated; the CGCs of **P7** in mixtures with 25 and 30% THF were very low, ~0.1% (i.e., corresponding to one molecule of **P7** immobilizing >1700 molecules of THF and >22200 molecules of water! The CGCs of **P4** and **P8** in almost all of the liquid mixtures gelated were >1.0%.

All of the gels at 2.0% **Pn**, except those in the liquid mixtures with extremely high water contents, were stable and of no syneresis at room temperature for at least three months when stored in sealed tubes. The gels with very high water compositions, such as those of **P4**, **P7**, and **P8** in 90% water and **P6** in 80% water, underwent phase separation within ~1 month after being made. The "thermostability" of a gel can be

Table 1. Appearances, T_{gel} Values (°C) of Gels of 2% Pn, and CGCs (%; in parentheses) of Pn in v:v THF:Water Mixtures at Room Temperature[a]

THF:H₂O	P2	P3	P4	P6	P7	P8
100:0	I	I	I	I	I	I
95:5	Sus S^b	Sus S^b	S	S	S	S
90:10−50:50	S	S	S	S	S	S
45:55	S	S	S	S	G 43.5−44.5 (1.7)	S
40:60	S	S	S	S	G 44−46 (1.8)	G 43 (1.4)
35:65	S	Sus S^b	G 34−35 (1.6)	G 45.5−46.5 (0.6)	G 48−49 (1.0)	G 43−44 (1.6)
30:70	Sus P^b	Sus S^b	G 36−37 (1.4)	G 46−47 (0.5)	G 50−51 (0.1)	G 50−51 (0.9)
25:75	I P^b	Sus P^b	G 37−38 (1.4)	G 49 (0.6)	G 49.5−50 (0.1)	G 42−43 (1.1)
20:80	I P^b	Sus P^b	G 40−41 (0.9)	G 49−50 (0.5)	G 49−50 (0.4)	G 44−46 (0)
15:85	I P^b	I P^b	G 35−36 (1.3)	G 49−50 (0.5)	G 46.5−47.5 (0.7)	G 42 (1.5)
10:90	I P^b	I I^b	G 36−37 (1.3)	Sus Sus^b	G 40 (0.8)	G 42−43.5 (1.4)
5:95	I I^b	I I^b	Sus Sus^b	Sus Sus^b	Sus Sus^b	I Sus^b
0:100	I	I	I	I	I	I

[a]G = gel, S = clear and transparent solution/sol, I = insoluble, Sus = suspension, PG = partial gel; see Experimental Section for explanations. Samples were prepared without heating unless indicated [b]sample heated to ca. 60 °C in a water bath and cooled to room temperature in air.

described by its specific solution/sol-to-gel or gel-to-solution/sol phase transition temperature (T_{gel}). The data in Figure S3 show that the T_{gel} values in several selected liquid mixtures increased with increasing **P7** concentration up to ~2% and then reach a "plateau" value. Thus, we compared the T_{gel} values at 2.0% of the other **Pn** as a function of THF:water composition (Figure S4). The T_{gel} values of the gels of **P4**, **P7**, and **P8** increased and then decreased with increasing THF composition and reached maximum values at 20%, 30%, and 30% THF compositions, respectively. The T_{gel} values of 2.0% **P6** gels decreased only slightly upon increasing the THF composition.

Self-Assembly Behavior and Liquid Polarity Assessed by the $E_T(30)$ Scale. In general, if the polarity of a solute molecule is similar to that of a liquid, they are expected to be miscible (i.e., "likes dissolve likes"). In that regard, the gelation process can be considered to be a balance between aggregation and dissolution of a gelator in a liquid.[15] To understand better the correlation between the polarity of a liquid mixtures and the self-assembly behaviors of the **Pn**, the maximum absorption wavelengths (λ_{max}) and $E_T(30)$ values of Reichardt's dye (Chart S1) in THF:water mixtures were measured (Figure 2). $E_T(30)$
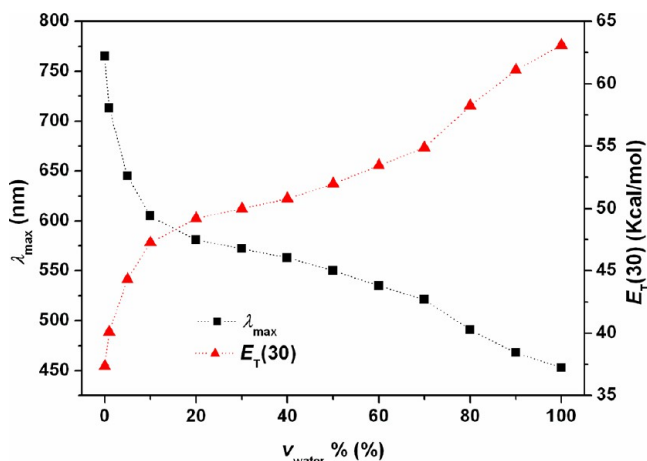

Figure 2. Maximum absorption wavelengths (λ_{max}) and $E_T(30)$ values of Reichardt's dye, calculated according to eq 4, as a function of THF:water compositions.

is a measure of liquid polarity (eq 4); high $E_T(30)$ values correspond to higher polarities.[34] According to this (and other) scales, the polarity of THF ($E_T(30) = 37.4$ kcal/mol) is much lower than that of water ($E_T(30) = 63.1$ kcal/mol). $E_T(30)$ increases sharply when even 1−10% water is added to THF and more slowly thereafter at higher water compositions. The observation that the **Pn** could not be dissolved in either neat THF or neat water but was dissolved or formed gels in some mixtures of them may be a consequence of the polarity of the **Pn** molecules being close to that of some liquid mixtures or to selective solvation of the different functional groups by each liquid component. If the overall **Pn** polarities are near the *average* polarities of the liquids in which they dissolve, the liquid mixture with 35%, 37.5%, 32.5%, 32.5%, 27.5%, and 30% water are similar to the polarities of **P2**, **P3**, **P4**, **P6**, **P7**, and **P8**, respectively. For example, 5−65% water in the liquid mixtures can dissolve **P2** well (Table 1). Thus, the presumed average polarity of these liquid mixtures, near 35%, is taken to be like the polarity of **P2**. Although the differences among the **Pn** values must be related to the lengths of the spacers connecting the pyrenyl and glucono groups, there is no obvious

progression. Other factors, such as the conformations adopted by the molecules with different spacers, may be important as well. Regardless, as the composition of water is increased to ~60−85%, the polarities of the mixtures appear to differ sufficiently from those of the **Pn** to force aggregation. Above a polarity limit (i.e., at very high water compositions), the aggregation processes for the **Pn** do not support gelation due to interfacial energy disparities, and the **Pn** precipitate in macroscopic forms or do not dissolve.

Self-Assembly Behavior and HSPs. In an attempt to dissect in greater detail than is possible with the $E_T(30)$ scale the factors related to the dissolution of, gelation by, and precipitation of the **Pn** in the liquid mixtures, we have calculated and compared the HSPs of the solvent mixtures and the **Pn**. Table S2 summarizes the HSPs of the liquid mixtures.[36] For example, the Hansen space of **P7** was fitted using "The Independent Sphere Fit Method" of the Hansen Solubility Data Fitting Software[33,37] (Figure S5). The polar interaction parameter (δ_p) and hydrogen-bonding interaction parameter (δ_h) of the liquid mixtures cover a large portion of Hansen space, while the dispersive interaction parameter (δ_d) remains within a very narrow range ($15.5 \leq \delta_d \leq 16.8$ MPa$^{0.5}$). Points for solutions/sols are included in one sphere, gels in another sphere, and suspensions or insoluble mixtures outside the spheres. However, δ_p, δ_h, and δ_d of the centers of the two spheres for **P7** were found to differ: for the solution sphere, $\delta_p = 8.36$ MPa$^{0.5}$, $\delta_h = 16.89$ MPa$^{0.5}$, and $\delta_d = 16.46$ MPa$^{0.5}$; and for the gel sphere, $\delta_p = 13.11$ MPa$^{0.5}$, $\delta_h = 32.73$ MPa$^{0.5}$, and $\delta_d = 15.87$ MPa$^{0.5}$. To avoid additional complications, the Hansen space was refitted using "The Concentric Sphere Shell Fit Method" of the Hansen Solubility Data Fitting Software.[33,38] The data are shown in Figure 3 for **P7** and in Figures S6−S10 for the other **Pn**. In the Hansen spaces, the solution spheres (blue) are nearest the center, the gel shells (green) are next, and the insoluble shells (red) are outermost. In most cases, the individual liquid mixtures fit within their proper spheres/shells.

The Hansen spaces of **P4−P8** are similar as a consequence of their similar gelation behaviors in the liquid mixtures, while
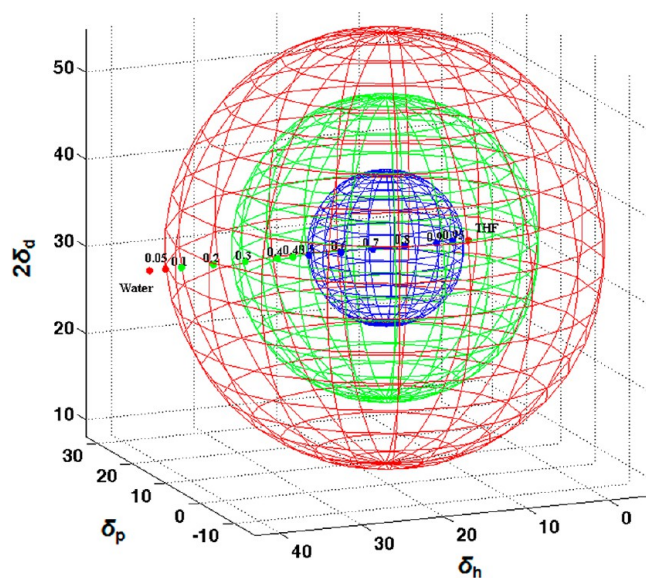

Figure 3. Solubility data for 2.0% **P7** in liquid mixtures represented in Hansen space with spheres/shells: blue (soluble), green (gel), and red (insoluble).

those of **P2** and **P3** belong to the other family. There are no gel points for **P2** and **P3**; instead, there are more insoluble points compared with those of the spheres/shells for **P4–P8**. By this model, the three spheres/shells are forced to share the same center in Hansen space. The radius (R_{sol}) of the solution sphere of each **Pn**, the individual HSPs for each **Pn**, the water composition of the liquid mixture whose HSPs are closest to those of a **Pn**, and the water composition of the mixture whose polarity is most similar to that of a **Pn** according to the $E_T(30)$ scale are summarized in Table 2. As expected based upon the

Table 2. Radii (R_{sol}, MPa$^{0.5}$) of the Solution Sphere, Individual HSPs (MPa$^{0.5}$) for the Pn, and the Composition of the Liquid Mixture Which Has the Closest HSPs and Polarity to Those of a Pn from Hansen Space and $E_T(30)$ Values

Pn	R_{sol}	δ_p	δ_h	δ_d	% water (from Hansen space)	% water (from $E_T(30)$ values)
P2	10.20	10.20	22.54	15.64	42	35
P3	9.70	10.10	20.52	16.56	37	37.5
P4	10.40	9.18	19.61	16.36	34	32.5
P6	10.40	9.18	19.61	16.36	34	32.5
P7	8.80	8.36	16.89	16.46	26	27.5
P8	9.10	8.79	18.32	16.41	30	30

data presented thus far, the individual HSPs for **P2** and **P3** are very similar, while those for **P4–P8** are near each other (but different from those of **P2** and **P3**!). Generally, if the distance (R) between a liquid point and the center of the solution sphere is smaller than the empirical (and case-specific) value of R_{sol}, the gelator and the liquid are expected to be miscible, and if R is larger than R_{sol}, the gelator is expected to undergo a form of phase separation from the liquid.[39,40] From the results in Tables 2 and S2, R_{sol} for **P7**, 8.80 MPa$^{0.5}$, which is larger than the R of the liquid mixtures with 5–50% water but smaller than

those of neat THF and the liquid mixtures with 55–100% water (as expected from the correlation between the gelation properties and liquid polarity). Furthermore, the results in Table 2 show that the individual HSPs of each **Pn** are very close to those of a liquid mixture. For example, those of **P7** are close to the values of the liquid with 26% water (δ_p = 8.38 MPa$^{0.5}$, δ_h = 16.94 MPa$^{0.5}$, and δ_d = 16.46 MPa$^{0.5}$). The most compatible compositions calculated from Hansen space and $E_T(30)$ values are quite similar for all of the **Pn** except **P2** (Table 2). These results provide a more quantitative measure of the degree to which the polarities of a **Pn** and a liquid must differ in order to induce aggregation (including gelation) of macrophase separation. They also identify the specific interaction factors which are most responsible for the observed nature of the **Pn**-liquid mixtures, and indicate again that the sufficient self-assembly behaviors of **Pn** in the liquid mixtures are induced by the difference between the Hansen solubility parameters and the polarity of **Pn** and the liquid mixtures of THF and water.

Individual HSPs, overall HSPs, and distances in Hansen spaces from **Pn** with its CGCs in the gelated liquid mixtures are correlated in Figure S11–S14. As opposed to the good correlations found between the CGCs of the **Pn** and the HSPs of 30 neat liquids,[17] no obvious correlation can be discerned with the THF:water mixtures. Although the CGCs changed with increasing HSPs and R distances, neither parameter appears to have a clear effect on the gelating ability of **P7**, and the trend in a plot of δ_d versus the CGCs (Figure S10c) is different from those of the other HSPs (Figure S10a,b,d,e). Similar results were found for the other **Pn** (Figures S11–S13). Thus, although the analyses using Hansen parameters provide important insights into the factors affecting solubilization and gelation of the **Pn**, they do not lead to conclusions which may be applied directly to other LMMG systems. The reasons for an *a priori* inability to extrapolate the conclusions for the **Pn** gelators to other systems involve the potential importance of factors other than the ones included in
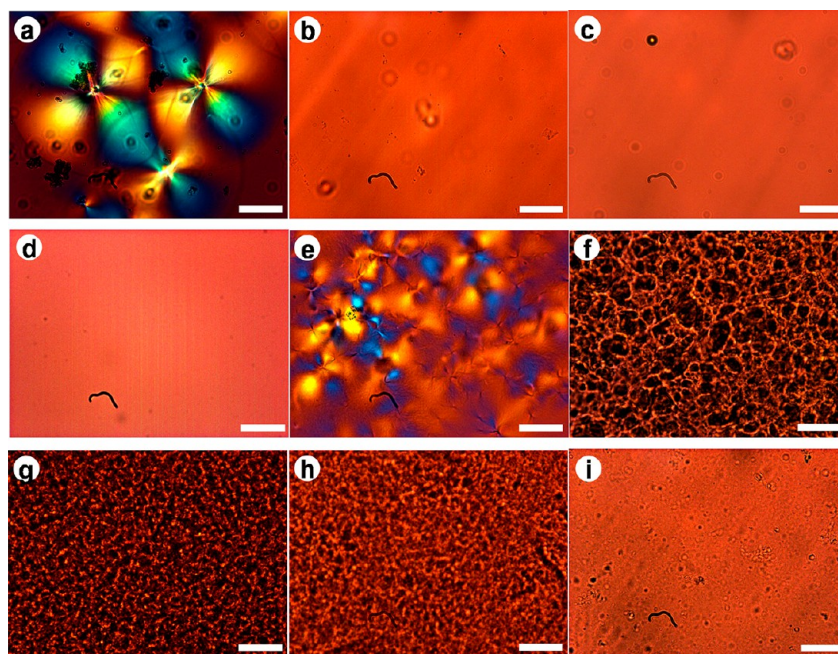

Figure 4. POMs (full-wave plate) of 2.0% **P7** in THF:water mixtures: (a) gel, 100:0; (b) solution/sol, 95:5; (c) solution/sol, 70:30; (d) solution/sol, 50:50; (e) gel, 40:60; (f) gel, 30:70; (g) gel, 25:75; (h) gel, 20:80; (i) suspension, 0:100. (Distance bars =100 μm).

the HSPs polarity, hydrogen bonding, and dispersive forces. For example, the interactions between a gelator molecule and the component species of a mixed solvent may be selective for one of the components, so that the properties of the bulk are not representative of the local solvation. In fact, this situation is probably occurring in our systems, where the glucono part of a **P***n* molecule is more attracted to water and the pyrenyl part prefers to be near THF.

Morphology Studies. POM images of solutions/sols, gels, and suspension of 2.0% **P7** in liquid mixtures with different compositions have been compared in Figure 4. The results demonstrate, as expected, that the morphologies of the **P***n* depend upon the compositions of the liquid mixtures.[41] The aggregates of the gel of **P7** in neat THF, made by heating to dissolve the gelator and then cooling the solution/sol, were star-like in appearance (Figure 4a). In the clear solutions/sols of **P7** in liquids with 5−50% water, prepared at room temperature, no microphase-separated aggregates could be detected (Figures 4b−d). In compositions with 55−90% water, again prepared without heating, aggregates from the stable gels were seen clearly (Figures 4e−h), and the degree of aggregation increased with increasing water content. In the suspension of **P7** in neat water at room temperature, only some small insoluble particles were observed (Figure 4i). The POM images of gels of 2% **P4**−**P8** in 20:80 THF:water mixture are shown in Figure S15. Although they are somewhat similar, distinct differences are apparent.

The SEM images of the solids from the solutions/sols of 2.0% **P7** in 95:5, 70:30, and 50:50 THF:water mixtures and the xerogels from gels of 2.0% **P7** in 40:60, 30:70; 25:75, and 20:80 THF:water mixtures are shown in Figure S16. Although the method of removal of the liquid components may result in a change in the **P7** network structures of the gel or (especially) solution/sol states, the changes in the dimensions of the layer-like structures are consistent with the POM images—they increase with increasing water content—indicating again that the degree of aggregation increases with increasing water content.

Pyrene dissolves readily in low-polarity liquids, and glucose dissolves easily in water; thus, the **P***n* are uncharged surfactants. As stated above, 2% **P7** forms transparent solutions/sols in 95:5, 70:30, and 50:50 THF:water mixtures at room temperature. In an attempt to detect aggregates of **P7** in these solutions/sols, confocal microscopy images and DLS measurements were taken on the transparent solutions/sols of 0.2% (3.5×10^{-3} M) and 2% (3.5×10^{-2} M,) **P7** in 95:5, 70:30 and 50:50 THF:water mixtures. Although, no clear images were obtained from confocal microscopy, the DLS measurements (Figure S17) indicated the presence of particles of 60−290 nm diameter with a maximum distribution at 130 nm for the solution/sol of 0.2% (3.5×10^{-3} M) **P7** in 95:5 THF:water (Figure 5 and Table S3).[42] Consistent with the SEM results for solutions/sols (Figure S16a−c), the average size and the breadth of the distribution (as indicated by the full widths at half height in Figure 5) of the **P7** aggregates increased with increasing concentration in one liquid mixture or with larger water content at one **P7** concentration (Figure 5 and Table S3). Note also the absence of detectable scattering from either 95:5 or 70:30 mixtures at 1.1×10^{-5} and 1.1×10^{-4} M **P7** (Table S4); these four samples cannot contain large aggregates. However, for the systems in 50:50 THF:water mixtures at the same two **P7** concentrations, significant scattering was observed, and the diameters at the maxima of the distribution
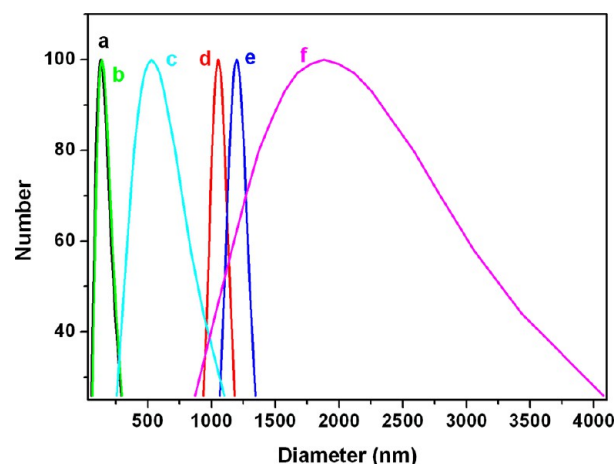

Figure 5. Distributions of diameters of the scattering particles in the solutions/sols of 0.2% (3.5×10^{-3} M) **P7** in 95:5 (a), 70:30 (b), and 50:50 (c) THF:water mixtures and of 2.0% (3.5×10^{-2} M) **P7** in 95:5 (d), 70:30 (e), and 50:50 (f) THF:water mixtures at 25 °C.

curves are 500 and 520 nm, respectively. In this regard, it is important to remember that gels are found in 45:55 THF:water mixtures at higher **P7** concentrations.

Packing Arrangements from XRD Studies. XRD was employed to investigate the dependence of packing motifs on the liquid composition. The XRD patterns of the neat powder and gels of **P7** are compared in Figure S18, and the corresponding *d* values of the diffraction peaks have been calculated from the Bragg equation (Table S5). The diffraction peaks of the **P7** component in the gels were identified by subtracting empirically the amorphous scattering of the liquid mixture from those of the gel diffractograms.[43] The diffractogram of neat **P7** (Figure S18a) can be indexed to monoclinic lattices.[17] The packing arrangement of **P7** in its gels is less clear, especially **P7** in 20:80 THF:water where one small peak with a *d* value of 4.16 nm and several other small peaks at higher angles (smaller distances) could be identified. However, the gross appearances of the neat solid and gel diffractograms are very similar (Table S5), and all contain a lowest angle peak corresponding to a *d* value of 4.16 nm. We suggest that the molecular packing arrangements of **P7** in the neat powder and gel phases are very similar. Because the calculated end-to-end distance of an interdigitated dimer of **P7**, including the van der Waals radii of the terminal atoms, is 4.36 nm (Figure S19),[17] the low-angle peaks corresponding to 4.16 nm in the diffractograms are consistent with lamellar packing arrangements. In that regard, note the similarity of the POM images in Figure 4f−h and the SEM images in Figure S16d,e.

Spectroscopic Studies. **P7** at 2% cannot be dissolved completely in neat THF or in neat water at room temperature; the mixtures of **P7** in neat THF or in neat water consist of liquid and insolubilized **P7** solid. The concentrations of dissolved **P7** in these liquid portions of these mixtures were calculated from Beer's law and assuming the molar extinction coefficients from the liquids in which all of the **P7** was dissolved. They are about 2.1×10^{-3} M in neat THF or 3.3×10^{-4} M in neat water (see Experimental Section). **P7** at 0.15% (2.6×10^{-3} M) can be dissolved well in 95:5−40:60 and 20:80 THF:water mixtures and forms a gel in 30:70 THF:water mixture. At <~1.1×10^{-4} M concentrations, **P7** can be dissolved in neat THF, neat water, and all compositions of their mixtures.

In order to investigate the changes in the self-assembly of **P7** in THF:water mixtures, UV–vis absorption spectra of **P7** in THF:water mixtures were recorded at different concentrations (Figure S20). The peaks in the spectra of the clear solutions/sols and transparent gels of **P7** at these concentrations were bathochromically shifted and lost some intensity as water was added. Such changes are consistent with increasing aggregation and π–π stacking of pyrenyl moieties.[17,44,45] Note also that the $S_0 \rightarrow S_1$ (>310 nm) absorption band[46,47] in Figure S20 changed very little, but the $S_0 \rightarrow S_2$ ($250 < \lambda < 310$ nm) absorption band did change markedly as the fraction of water in the mixtures was increased (Figures S20 and 6); as expected on the basis of
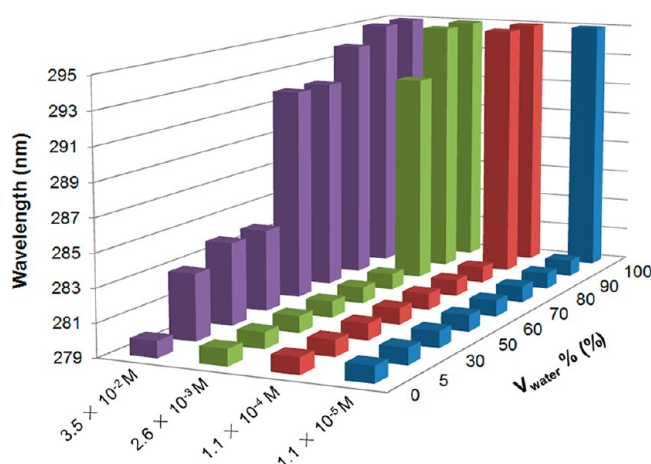
Figure 6. Shifts of the wavelength maximum for the $S_0 \rightarrow S_2$ absorption band ($250 < \lambda < 310$ nm) of **P7** at different concentrations and THF:water compositions.

dielectric constants and as demonstrated by the $E_T(30)$ values (Figure 2), the polarity of the THF:water mixtures increases with increasing water content. Thus, we suggest that the variation in $S_0 \rightarrow S_2$ band might be related to its greater sensitivity than the $S_0 \rightarrow S_1$ transition to solvent polarity. Moreover, absorption spectra of 3.5×10^{-2} M **P7** exhibited bathochromic shifts of the $S_0 \rightarrow S_2$ absorption band when even 5% water was added to THF (Figure 6); consistent with the conclusions from DLS measurements, **P7** molecules at relatively high concentrations aggregate even in solvent mixtures with very low water contents. Note also that the relatively large increase in the bathochromic shift between 50% and 60% water at 3.5×10^{-2} M is consistent with the observed phase change from solution/sol to gel at these compositions.

Fluorescence measurements have been used as well to probe changes in the self-assembly of **P7**. The fluorescence emission spectra of the liquid phases from the mixtures of 2% **P7** in neat THF (dissolved $[\textbf{P7}] = 2.1 \times 10^{-3}$ M) or in neat water (dissolved $[\textbf{P7}] = 3.3 \times 10^{-4}$ M), and the spectra of the clear solutions/sols and the gels of 2% (3.5×10^{-2} M, total concentration) **P7** (Series B) in THF:water mixtures are compared in Figure 7. All of the spectra (except those in 10:90 THF:water and in neat water) included structured peaks from monomeric pyrenyl singlet states and a broad band from an excimeric emission. The profiles of the emission of **P7** in the mixtures from 100:0 to 20:80 THF:water evolved gradually but differ significantly from those in 10:90 and in 0:100 THF:water (consistent with the changes in the $S_0 \rightarrow S_2$ absorption band noted in Figure 6).
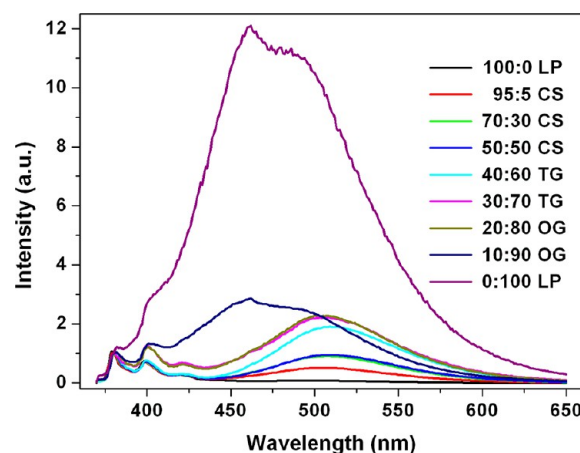

Figure 7. Fluorescence spectra (λ_{ex} 350 nm; intensity normalized at 379 nm) of the liquid phases from mixtures of 2% **P7** in neat THF ($\sim 2.1 \times 10^{-3}$ M) or in neat water ($\sim 3.3 \times 10^{-4}$ M) and the spectra of the solutions/sols and the gels of 2% (3.5×10^{-2} M) **P7** (Series B) in THF:water mixtures at 20 °C. Appearances of the samples: LP = liquid phase, CS = clear solution/sol, TG = transparent gel, OG = opaque gel.

The increase in relative intensity at the wavelength maximum of the excimeric emission (~500 nm) with increasing water content is another very strong indicator of aggregation of pyrenyl groups. Because **P7** is only slightly soluble in THF at room temperature, the relative intensity of the excimeric emission is low; the $I_{379\ nm}/I_{500\ nm}$ intensity ratio is 13.21 (Table S6). By contrast, the $I_{379\ nm}/I_{500\ nm}$ intensity ratio in 95:5 THF:water is 1.98, and it decreases gradually with increasing water content (to 0.93 in 50:50 THF: water; Table S6). Note also that the maximum emission wavelengths of the excimeric emissions of **P7** in 10:90 THF:water and in neat water, 462 nm, are blue-shifted by ~40 nm with respect to those of 'normal' pyrenyl excimer emissions[42,48] or to those with higher THF contents. One possible explanation for this hypsochromic shift is that neighboring pyrenyl units in an aggregate are unable to attain the relaxed excimeric geometry within their excited-state lifetimes in the primarily aqueous liquids. Moreover, aggregation has the effect of shielding the pyrenyl units from water and thus creates a microenvironment which is less polar than that of the bulk solvent. A lower average polarity of the microenvironment experienced by the pyrenyl groups of **P7** in the liquid mixtures is indicated by the I_1/I_3 vibronic band intensity ratios of the monomeric component of the emission: the ratios for **P7** are 1.45 in THF and 0.41 in water (Table S6); the I_1/I_3 ratio of pyrene is reported to be 1.35 in neat THF and 0.41 in its vapor phase.[49] The I_1/I_3 ratios were also calculated by two methods which were intended to remove the effect of competing excimeric emissions at the wavelengths of interest (see Experimental Section). Although the I_1/I_3 ratios from the treatments differ somewhat, the trends with the polarities of the THF:water mixtures are the same (Figure S21). Overall, these data are consistent with the observations from DLS measurements (Figure 5d–f) that larger aggregates form as the water content increases.

The maximum wavelengths of the excitation spectra of 2.0% **P7** are bathochromically shifted progressively from 378 nm in THF to 392 nm in water as the water content is increased (Figure S22). The possible reasons for spectral changes discussed above are consistent with the data in the excitation
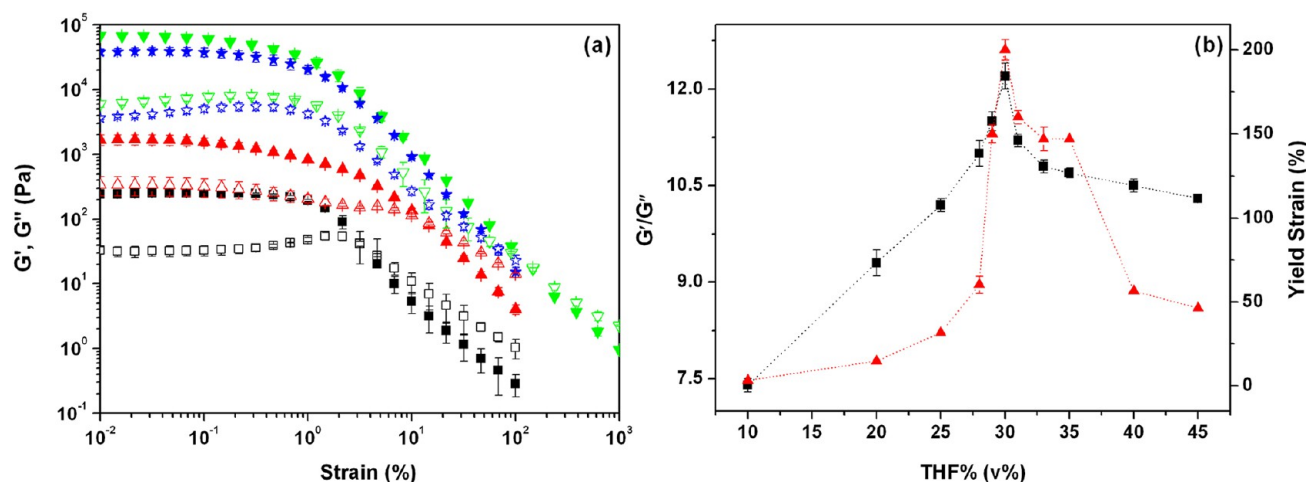
8996

dx.doi.org/10.1021/ja402560n | *J. Am. Chem. Soc.* 2013, 135, 8989−8999

Figure 8. (a) Log−log strain sweep (frequency =1.0 Hz) for gels of 2.0% **P7** in (■) 10:90, (▲) 20:80, (▼) 35:65, and (★) 45:55 THF:water mixtures at 25 °C. G' (closed symbols) and G'' (open symbols). (b) Plot of G'/G'' (■) at strain =0.01% and yield strain (▲) versus % THF in 2.0% **P7** in THF:water gels at 25 °C. One standard deviation of data from three trials is shown.
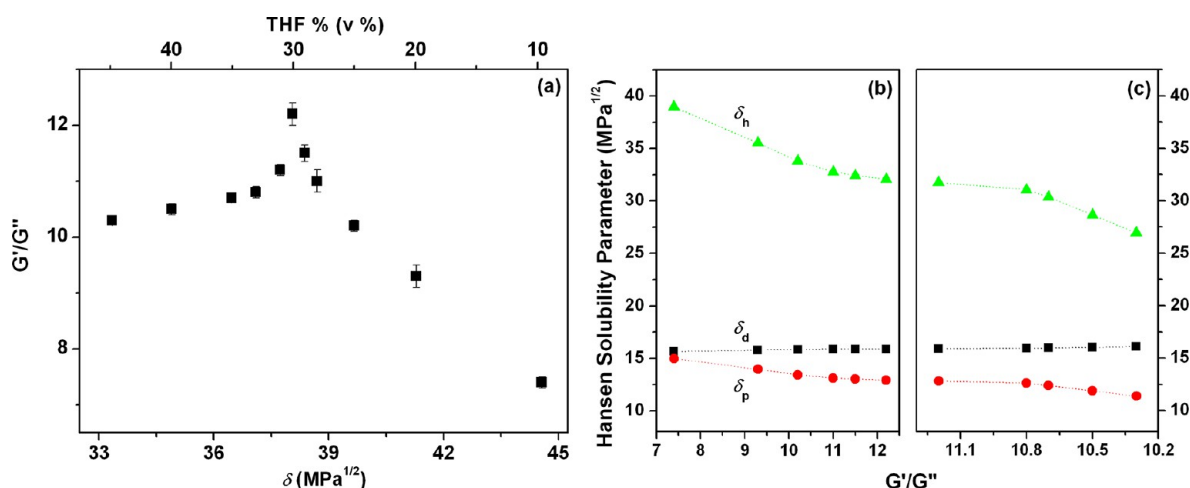

Figure 9. Effect of the overall Hansen solubility parameter (δ) and THF content (a) and the individual Hansen solubility parameters (b and c) on G'/G'' (at strain = 0.01%) from gels of 2% **P7**.

spectra as well. The results indicate that aggregation of pyrenyl groups of **Pn** increases with increasing water content and $\pi-\pi$ stacking is one of the important driving forces for aggregation.

Rheology of the Gels. The mechanical properties of 2.0% **Pn** gels were investigated as a function of THF:water composition (Figures 8 and S23−S25). The rheological properties of samples with **P2** or **P3** were not examined because they were not gel-like, even after heating and cooling, according to the simple inversion test. The storage moduli (G'), loss moduli (G''), G'/G'' ratios (in the linear viscoelastic region at strain = 0.01%), and yield strains reported from strain sweeps of each **Pn** sample are the average from three different aliquots (Tables S7−S10).

Figure 8a shows results from gels of 2.0% **P7** in different liquid mixtures. In all of the samples, the initial G' is higher than G'' by about 1 order of magnitude and remains higher over large ranges of strain. This is the comportment expected of a true gel phase.[50,51] With a gradual increase in applied strain, both G' and G'' remain almost invariant (i.e., in the linear viscoelastic region), and at a certain yield strain, they cross, indicating a mechanical break of the gel structures; beyond the yield strain, the G'/G'' values deviate from linearity. From the

results in Figure 8b and Table S7, both G'/G'' at strain = 0.01% and the yield strain increase and then decrease with increasing THF composition and reach a maximum mechanical stability (G'/G'' = 12.2 ± 0.2; yield strain = (200 ± 6)%) in the 30:70 THF:water gel.[52] This composition was observed to have the highest thermostability (T_{gel} = 50−51 °C, Figure S4) and lowest critical gelation concentration (0.1%, Figure S2).

In gels of the other **Pn**, both G'/G'' at the initial strain and the yield strain increase and then decrease with increasing THF composition (Figures S23−S25). The maximum values of G'/G'' and yield strains of the **P4**, **P6**, **P7**, and **P8** gels occur at 20%, 32%, 30% and 33% THF contents, respectively.

Gels of 2% **P7** in 6 THF:water compositions were subjected to frequency sweep measurements. The values of G' of the samples are nearly constant over a frequency range of 0.01 to 100 Hz and remain greater than their associated G'' (Figure S26a). This behavior is typical of a gel[50] (albeit a weak one, given the absolute magnitudes of G'; for example, G' of 2% **P7** in the 35:65 THF:water gel is ~52000 ± 12000 Pa at 1 Hz). The values of G'/G'' at 1 Hz follow a similar trend (Figure S26b) to that in Figure 8b; again, the most stable **P7** gel appears to be at 30% THF.

Gel Rheology and HSPs. Table S11 and Figure 9 show the correlation between the HSPs of the liquid mixtures and the values of G'/G'' at strain = 0.01% of 2% **P7** gels. Similar results were found for gels with the other **Pn** (Figures S27−S29). G'/G'' for the **P7** gels displays a sharp maximum at an overall Hansen solubility parameter (δ = 38.06 MPa$^{0.5}$) corresponding (again!) to 30% THF content.[32] Although no maxima are observed when the individual components of the Hansen parameters are plotted versus G'/G'', the major contributor to changes is the hydrogen-bonding interaction parameter, δ_h (Figure 9b,c).

CONCLUSIONS

The unexpected self-assembly behavior of a series of fluorescent **Pn** LMMGs have been found to yield viscoelastic gels in a wide range of THF:water mixtures and solutions/sols in others despite the fact that 2% **Pn** is insoluble at room temperature in either neat THF or neat water. The nature of the self-assembly processes, determined by a variety of techniques, has led to an understanding of the relationship between the properties of the **Pn** aggregates and those of the THF:water mixtures. Thus, the compositions of the THF:water mixtures determine **Pn** particle size in solutions/sol phases, critical gelation concentrations, microstructures, thermo- and mechanical stabilities of the gels, and the molecular packing modes of the **Pn** molecules in their gel networks. The packing of the molecules within their gel networks involves extensive $\pi-\pi$ stacking and H-bonding, perhaps in interdigitated lamellae which are fiber-like on a micrometer length scale.

Both the $E_T(30)$ polarity scale and Hansen solubility parameters produce information which is well-correlated with the comportment of the **Pn** in the liquid mixtures. The compositions which yield gels or solutions/sols or cannot dissolve the **Pn** are predicted reasonably well by these treatments. A detailed analysis of the components of the Hansen parameters and rheology measurements suggests that hydrogen-bonding interactions are a major factor in determining the mechanical stability of the gels. Specifically, the methodology employed here allows the balance between dissolution and aggregation of **Pn** molecules in the liquid mixtures to be analyzed in great detail. The fact that the correlations are not 'perfect' indicates that factors not included in these treatments must be operating as well.

A very important aspect of this approach is its applicability to dissect the factors controlling the balance between aggregation and dissolution of LMMGs with very different molecular structures as well as with molecules which form micelles, vesicles, and other aggregates. We intend to explore new liquid mixtures in which the strategy can be used for other surfactant-like LMMGs to construct systems with predefined self-assembly properties and to probe the additional factors which control molecular aggregation.

ASSOCIATED CONTENT

⑤ Supporting Information

Synthesis and characterization of **Pn**, Hansen spaces of **Pn** in 30 liquids, the correlation of Hansen solubility parameter and CGCs, XRD patterns, rheological data, and additional spectra and images. This material is available free of charge via the Internet at http://pubs.acs.org.

AUTHOR INFORMATION

Corresponding Author

yfang@snnu.edu.cn; weissr@georgetown.edu

Notes

The authors declare no competing financial interest.

REFERENCES

(1) Yang, Y. G.; Suzuki, M.; Shirai, H.; Kurose, A.; Hanabusa, K. *Chem. Commun.* **2005**, 2032−2034.
(2) Dowling, T. C.; Arjomand, M. A.; Lin, E. T.; Jr, L. V. A.; McPherson, M. *Am. J. Health-Syst. Pharm.* **2004**, *61*, 2541−2544.
(3) Zhang, M. M.; Sun, S. T.; Yu, X. D.; Cao, X. H.; Zou, Y.; Yi, T. *Chem. Commun.* **2010**, *46*, 3553−3555.
(4) Terech, P.; Weiss, R. G. *Chem. Rev.* **1997**, *97*, 3133−3159.
(5) Žinic, M.; Vögtle, F.; Fages, F. *Top. Curr. Chem.* **2005**, *256*, 39−76.
(6) Sangeetha, N. M.; Maitra, U. *Chem. Soc. Rev.* **2005**, *34*, 821−836.
(7) Weiss, R. G.; Térech, P. In *Molecular gels. Materials with self-assembled fibrillar networks*; Weiss, R. G.;Térech, P., Eds.; Springer: Dordrecht, 2006, pp 1−13.
(8) Ran, X.; Wang, H.; Zhang, P.; Bai, B.; Zhao, C.; Yu, Z.; Li, M. *Soft Matter* **2011**, *7*, 8561−8566.
(9) Cravotto, G.; Cintas, P. *Chem. Soc. Rev.* **2009**, *38*, 2684−2697.
(10) Dawn, A.; Shiraki, T.; Ichikawa, H.; Takada, A.; Takahashi, Y.; Tsuchiya, Y.; Lien, L. T. N.; Shinkai, S. *J. Am. Chem. Soc.* **2012**, *134*, 2161−2171.
(11) Kar, T.; Debnath, S.; Das, D.; Shome, A.; Das, P. K. *Langmuir* **2009**, *25*, 8639−8648.
(12) Suzaki, Y.; Taira, T.; Osakada, K. *J. Mater. Chem.* **2011**, *21*, 930−938.
(13) Gasnier, A. l.; Royal, G.; Terech, P. *Langmuir* **2009**, *25*, 8751−8762.
(14) Kawano, S.-i.; Fujita, N.; Shinkai, S. *J. Am. Chem. Soc.* **2004**, *126*, 8592−8593.
(15) Estroff, L. A.; Hamilton, A. D. *Chem. Rev.* **2004**, *104*, 1201−1218.
(16) Yan, N.; He, G.; Zhang, H.; Ding, L.; Fang, Y. *Langmuir* **2010**, *26*, 5909−5917.
(17) Yan, N.; Xu, Z.; Diehn, K. K.; Raghavan, S. R.; Fang, Y.; Weiss, R. G. *Langmuir* **2013**, *29*, 793−805.
(18) Dastidar, P.; Okabe, S.; Nakano, K.; Iida, K.; Miyata, M.; Tohnai, N.; Shibayama, M. *Chem. Mater.* **2005**, *17*, 741−748.
(19) Ballabh, A.; Trivedi, D. R.; Dastidar, P. *Chem. Mater.* **2006**, *18*, 3795−3800.
(20) Sahoo, P.; Adarsh, N. N.; Chacko, G. E.; Raghavan, S. R.; Puranik, V. G.; Dastidar, P. *Langmuir* **2009**, *25*, 8742−8750.
(21) Cui, J.; Zheng, Y.; Shen, Z.; Wan, X. *Langmuir* **2010**, *26*, 15508−15515.
(22) Cai, X.; Liu, K.; Yan, J.; Zhang, H.; Hou, X.; Liu, Z.; Fang, Y. *Soft Matter* **2012**, *8*, 3756−3761.
(23) Xu, Z.; Peng, J.; Yan, N.; Yu, H.; Zhang, S.; Liu, K.; Fang, Y. *Soft Matter* **2013**, *9*, 1091−1099.

(24) Tamaru, S.-i.; Nakamura, M.; Takeuchi, M.; Shinkai, S. *Org. Lett.* **2001**, *3*, 3631−3634.

(25) Pal, A.; Dey, J. *Langmuir* **2011**, *27*, 3401−3408.

(26) John, G.; Jung, J. H.; Masuda, M.; Shimizu, T. *Langmuir* **2004**, *20*, 2060−2065.

(27) Xu, Y.; Xue, P.; Xu, D.; Zhang, X.; Liu, X.; Zhou, H.; Jia, J.; Yang, X.; Wang, F.; Lu, R. *Org. Biomol. Chem.* **2010**, *8*, 4289−4296.

(28) Chen, X.; Liu, K.; He, P.; Zhang, H.; Fang, Y. *Langmuir* **2012**, *28*, 9275−9281.

(29) Critchfield, F. E.; Gibson, J. A.; Hall, J. L. *J. Am. Chem. Soc.* **1953**, *75*, 6044−6045.

(30) George, M.; Funkhouser, G. P.; Weiss, R. G. *Langmuir* **2008**, *24*, 3537−3544.

(31) Brandrup, J.; Immergut, E. H.; Grulke, E. A. *Polymer Handbook*; 4 ed.; John Wiley & Sons: Hoboken, 2003.

(32) Appaw, C.; Gilbert, R. D.; Khan, S. A. *Biomacromolecules* **2007**, *8*, 1541−1547.

(33) Developed using MATLAB Compiler Runtime (MathWorks) as a platform. Available upon request from Kevin Diehn.

(34) Reichardt, C. *Chem. Rev.* **1994**, *94*, 2319−2358.

(35) Bondi, A. *J. Phys. Chem.* **1964**, *68*, 441−451.

(36) Hansen, C. M. *Hansen solubility parameters. A user′s handbook*, 2nd ed.; CRC Press: Boca Raton, FL, 2007.

(37) The independent sphere fit method fits every data class in its own Hansen sphere. The initial guess for the center of each class′ sphere is defined by the average of the data points making up that class.

(38) The concentric sphere shell fit method fits the data as concentric shells radiating out from the solution sphere. The initial guess for the solution sphere is defined by the average of the data points making up the solution class.

(39) Raynal, M.; Bouteiller, L. *Chem. Commun.* **2011**, *47*, 8271−8273.

(40) Gharagheizi, F. *J. Appl. Polym. Sci.* **2007**, *103*, 31−36.

(41) Wu, Y.; Wu, S.; Zou, G.; Zhang, Q. *Soft Matter* **2011**, *7*, 9177−9183.

(42) Abraham, S.; Weiss, R. G. *J. Am. Chem. Soc.* **2011**, *133*, 19250−19256.

(43) Ostuni, E.; Kamaras, P.; Weiss, R. G. *Angew. Chem., Int. Ed.* **1996**, *35*, 1324−1326.

(44) Babu, P.; Sangeetha, N. M.; Vijaykumar, P.; Maitra, U.; Rissanen, K.; Raju, A. R. *Chem.—Eur. J.* **2003**, *9*, 1922−1932.

(45) Korevaar, P. A.; Schaefer, C.; de Greef, T. F. A.; Meijer, E. W. *J. Am. Chem. Soc.* **2012**, *134*, 13482−13491.

(46) Búcsiová, L.; Hrdlovič, P.; Chmela, Š. *J. Photochem. Photobiol. A: Chem.* **2001**, *143*, 59−68.

(47) The actual origin of the vibronic bands at >310 nm and those centered near 250 nm may not be to the S_1 and the S_2 states, respectively. See, for example: Aschi, M.; Fontana, A.; Meo, E. M. D.; Zazza, C.; Amadei, A. *J. Phys. Chem. B* **2010**, *114*, 1915−1924.

(48) Adhikari, B.; Nanda, J.; Banerjee, A. *Chem.—Eur. J.* **2011**, *17*, 11488−11496.

(49) Dong, D.; Winnik, M. A. *Can. J. Chem.* **1984**, *62*, 2560−2565.

(50) Yao, S.; Beginn, U.; Gress, T.; Lysetska, M.; Würthner, F. *J. Am. Chem. Soc.* **2004**, *126*, 8336−8348.

(51) Piepenbrock, M.-O. M.; Lloyd, G. O.; Clarke, N.; Steed, J. W. *Chem. Rev.* **2009**, *110*, 1960−2004.

(52) Das, A.; Ghosh, S. *Chem.—Eur. J.* **2010**, *16*, 13622−13628.

How Do Liquid Mixtures Solubilize Insoluble Gelators? Self-Assembly Properties of Pyrenyl-Linker-Glucono Gelators in Tetrahydrofuran-Water Mixtures

Ni Yan,[†,‡] Zhiyan Xu,[†] Kevin K. Diehn,[§] Srinivasa R. Raghavan,[§] Yu Fang,[*,†] and Richard G. Weiss[*,‡,@]

[†]Key Laboratory of Applied Surface and Colloid Chemistry (Shaanxi Normal University), Ministry of Education, School of Chemistry and Chemical Engineering, Shaanxi Normal University, Xi'an 710062, P. R. China

[‡]Department of Chemistry and [@]Institute of Soft Matter Synthesis and Metrology, Georgetown University, Washington, DC 20057-1227, USA

[§]Department of Chemical and Biomolecular Engineering, University of Maryland, College Park, Maryland 20742-2111, USA

Table of Contents

---

[*] To whom correspondence should be addressed. E-mail: yfang@snnu.edu.cn (YF), weissr@georgetown.edu (RGW).

1. Synthesis of glucose-based pyrenyl-containing compounds

Materials: 1,3-Propanediamine (99+%), 1,4-butanediamine (99%), 1,7-heptanediamine (99%), 1,8-octanediamine (99%), and D-glucono-1,5-lactone (99%) were purchased from Alfa Aesar and used as received. Pyrene (Acros, 96%) was recrystallized from ethanol and then extracted with ethanol in a soxhlet extractor. 1,2-Ethylenediamine (analytical grade) was treated with solid KOH and distilled before use. All solvents and other chemicals used for syntheses were analytical grade and were purified by standard literature methods.

P2-P8, which are the final gelators with spacers containing 1,2-ethylenediamine, 1,3-propanediamine, 1,4-butanediamine, 1,6-hexanediamine, 1,7-heptanediamine, and 1,8-octanediamine, respectively, were synthesized by adopting literature methods as described below (Scheme S1).[1-3]
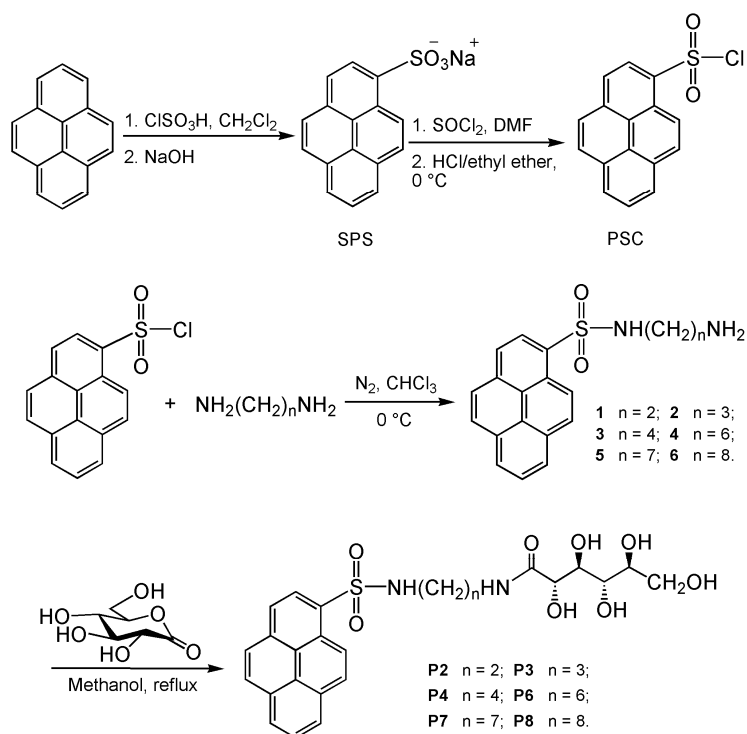
Scheme S1. Synthesis scheme for glucono-pyrenyl molecules (**Pn**).

(a) Synthesis of Sodium Pyrene-1-sulfonate (SPS):

Pyrene (4.85 g, 0.0240 mol) was dissolved in CH$_2$Cl$_2$ (30 mL). Chlorosulfonic acid (1.60 mL, 0.0240 mol), dissolved in CH$_2$Cl$_2$ (5 mL), was added drop-wise to the pyrene solution while stirring vigorously at 0 °C under a nitrogen atmosphere. Stirring was continued for a total of 2 h. The resulting dark-green solution was poured (*with extreme caution*) into ice (50 mL) and stirred in a beaker, allowing CH$_2$Cl$_2$ to evaporate in air at room temperature over a 2-day period. This solution was filtered twice through a Celite pad and the pad was washed with water (100 mL). The yellow

sodium salt of SPS was precipitated upon addition of NaOH (1.00 g, 0.0250 mol) to the filtrate. The solid was filtered and vacuum-dried (~ 1000 Pa) at 65 °C to yield 5.20 g (71%) of SPS sodium salt which was used in subsequent reactions without further purification.

(b) Synthesis of Pyrene-1-sulfonyl Chloride (PSC):

Dry hydrogen chloride was generated by adding concentrated sulfuric acid to sodium chloride and passing the gas through concentrated sulfuric acid before bubbling it through diethyl ether. The concentration of dissolved HCl, ~1 mol/L, was determined by adding 1 mL of the HCl/diethyl ether solution to ca. 10 mL of water followed by titration with a standard sodium hydroxide solution and phenolphthalein as the indicator. A 30 mL aliquot of the HCl/diethyl ether solution was added to a solution of SPS (9.10 g, 0.0300 mol) in DMF (200 mL) to generate the sulfonic acid. Thionyl chloride (22 mL, 0.18 mol) was then added dropwise under a nitrogen atmosphere. The reaction mixture was placed in an ice-water bath (~5 °C) for 3 h, and then the solution was poured into ice (400 mL). The yellow precipitate was filtered and washed with water (500 mL). The solid was air-dried overnight then vacuum-dried (~ 1000 Pa) at 55 °C for 12 h. The crude PSC was passed through a silica gel column with CH_2Cl_2 as eluent (R_f= 0.85) to yield 7.20 g (yield 80%) of PSC. Elemental analysis (EA) (%) calcd for PSC, $C_{16}H_9SO_2Cl$: C, 63.89; H, 3.00. Found: C, 63.60; H, 2.99.

(c) Syntheses of *N*-(1-Pyrenylsulfony1)alkyldiamines (**1**-**6**):

The *N*-(1-pyrenylsulfonyl)alkyldiamines were prepared from PSC and one of 1,2-ethylenediamine, 1,3-propanediamine, 1,4-butanediamine, 1,6-hexanediamine, 1,7-heptanediamine, or 1,8-octanedi-amine.

1,2-Ethylenediamine (4.50 mL, 0.0670 mol) was added to $CHCl_3$ (50 mL) and stirred rapidly at 0 °C under a nitrogen atmosphere. PSC (2.00 g, 6.60 mmol) was dissolved in $CHCl_3$ (300 mL) and added dropwise to the stirred diamine solution. After addition was completed (about 8 h), the mixture was brought to room temperature and stirred for another 2 h. The $CHCl_3$ layer was extracted with H_2O (6×200 mL) and 5% aqueous NaCl (250 mL), dried over anhydrous sodium sulfate, and filtered. The filtrate was evaporated under reduced pressure and the residue was dried in vacuum (~1000 Pa) to give **1** as a yellow solid (1.87 g, 80%). The procedures used for the preparation of **2**-**6** were similar to that for **1**. The yields for **2**-**6** were 75%, 78%, 75%, 80% and 70%, respectively.

(d) Syntheses of **P2**-**P8**:

D-glucono-1,5-lactone (0.940 g, 5.30 mmol) and compound **1** (1.72 g, 5.30 mmol) were dissolved in methanol (200 mL), and the mixture was stirred and refluxed in air for 10 h. The residue

obtained after the solvent was removed by evaporation was washed with chloroform (6×50 mL) to remove unreacted compound **1** and with water (6×50 mL) to remove unreacted lactone or species derived from it.   The remaining solid was dried in vacuum (~1000 Pa) to give a yellow powder (1.60 g, 60% yield), **P2**.   Analogous procedures were used for the preparations of **P3**, **P4**, **P6, P7** and **P8**.   However, the purification procedures for **P4**, **P6, P7** and **P8** were somewhat different.

To purify **P4**, 100 mL of water were added to the residue which had been washed with CHCl₃; the mixture became a very viscous suspension which could not be filtered.   NaCl solid (1 wt % of the coarse **P4**) was added to this suspension followed by centrifugation of the mixture at ~10,000 rpm for 30 min.   The supernatant liquid was removed and the solid was treated as above with aqueous NaCl 7 more times; between each centrifugation, the solid was collected and stirred in an aqueous NaCl solution for 30 min.   Finally, the solid was washed with water, centrifuged and dried in vacuum (~1000 Pa) to give **P4** as a yellow powder (1.68 g, 56% yield).   The procedures for the purification of **P6, P7** and **P8** are similar to that for **P4**.

For **P2**: 60% yield; mp 173.5-175 ℃. ^{1}H NMR (DMSO-d_6/Me$_4$Si, 300 MHz) δ (ppm): 8.97-9.00 (d, J = 9 Hz, 1H), 8.59-8.61 (d, J = 6 Hz, 1H), 8.20-8.50 (m, 8H), 7.75 (s, 1H), 5.33 (s, 1H), 4.30-4.52 (m, 4H), 3.86-3.92 (d, 2H), 3.45-3.55 (m, 4H), 3.10 (s, 2H), 2.88 (s, 2H). ^{13}C NMR (DMSO-d_6/Me$_4$Si, 100 MHz): δ 173.19 (1C, CO), 134.40, 132.69, 130.96, 130.40, 130.12, 129.98, 127.57, 127.54, 127.45, 127.37, 127.27, 127.15, 124.73, 124.67, 123.75, 123.61 (16C, ArC), 73.86, 72.69, 71.88, 70.39, 63.74 (5C, COH), 42.23, 38.61 (2C, CH$_2$).   FTIR (KBr) υ_{max} (cm^{-1}): 3407 (NH), 3533-3045 (OH); 3380 (HNSO$_2$); 2927 (CH); 1652 (C=O); 1533 (NH); 1415 (CN); 1309, 1151 (S=O).   EA (%) calcd for C$_{24}$H$_{26}$N$_2$O$_8$S·½H$_2$O: C, 56.35; H, 5.32; N, 5.48.   Found: C, 56.75; H, 5.11; N, 5.37.

For **P3**: 65% yield; mp 167-168.5 ℃. ^{1}H NMR (DMSO-d_6/Me$_4$Si, 300 MHz) δ (ppm): 8.97-9.00 (d, J = 9 Hz, 1H), 8.59-8.61 (d, J = 6 Hz, 1H), 8.19-8.50 (m, 7H), 8.10 (s, 1H), 7.63 (s, 1H), 5.33 (s, 1H), 4.32-4.54 (m, 4H), 3.87-3.95 (m, 2H), 3.38-3.56 (m, 4H), 3.00-3.01 (t, J = 3 Hz 2H), 2.51-2.86 (t, J = 6 Hz, 2H), 1.45-1.49 (t, J = 6 Hz, 2H). ^{13}C NMR (DMSO-d_6/Me$_4$Si, 100 MHz): δ 172.97 (1C, CO), 134.32, 133.09, 130.97, 130.33, 130.13, 129.89, 127.56, 127.50, 127.41, 127.38, 127.24, 127.06, 124.73, 124.68, 123.83, 123.63 (16C, ArC), 73.98, 72.80, 71.93, 70.47, 63.75 (5C, COH), 42.22, 35.99, 29.82 (3C, CH$_2$).   FTIR (KBr) υ_{max} (cm^{-1}): 3405 (NH), 3590-3050 (OH); 3396 (HNSO$_2$); 2933 (CH); 1646 (C=O); 1548 (NH); 1438 (CN); 1311, 1149 (S=O).   EA (%) calcd for C$_{25}$H$_{28}$N$_2$O$_8$S·½H$_2$O: C, 57.13; H, 5.56; N, 5.33.   Found: C, 57.07; H, 5.35; N, 5.31.

For **P4**: 56% yield; mp 131.8-133.5 ℃. ^{1}H NMR (DMSO-d_6/Me$_4$Si, 300 MHz) δ (ppm): 9.01-9.04 (d, J = 9 Hz, 1H), 8.60-8.62 (d, J = 6 Hz, 1H), 8.19-8.50 (m, 7H), 8.12 (s, 1H), 7.57 (s, 1H), 5.35 (s, 1H), 4.38-4.59 (m, 4H), 3.90-3.97 (m, 2H), 3.42-3.62 (m, 4H), 2.84-2.96 (b, 4H), 1.35-1.46 (b, 4H). ^{13}C NMR (DMSO-d_6/Me$_4$Si, 100 MHz): δ 172.71 (1C, CO), 134.29, 133.03, 130.95,

130.29, 130.12, 129.84, 127.53, 127.37, 127.20, 127.10, 127.05, 124.71, 124.63, 124.31, 123.90, 123.62 (16C, ArC), 74.04, 72.84, 71.92, 70.48, 63.78 (5C, COH), 42.57, 37.94, 26.85, 26.63 (4C, CH$_2$). FTIR (KBr) v_{max} (cm^{-1}): 3408 (NH), 3600-3072 (OH); 3380 (HNSO$_2$); 2935 (CH); 1639 (C=O); 1542 (NH); 1438 (CN); 1307, 1141 (S=O). EA (%) calcd for C$_{26}$H$_{30}$N$_2$O$_8$S·½H$_2$O: C, 57.87; H, 5.79; N, 5.19. Found: C, 57.30; H, 5.67; N, 5.30.

For **P6**: 60% yield; mp 127.0-129.5 ºC. ^{1}H NMR (DMSO-d_6/Me$_4$Si, 300 MHz) δ (ppm): 9.01-9.04 (d, J = 9 Hz, 1H), 8.60-8.63 (d, J = 9 Hz, 1H), 8.19-8.49 (m, 7H), 8.11 (s, 1H), 7.48 (s, 1H), 5.36 (s, 1H), 4.38-4.58 (m, 4H), 3.90-3.97 (m, 2H), 3.50-3.60 (m, 4H), 2.52-2.88 (b, 4H), 0.96-1.27 (m, 8H). ^{13}C NMR (DMSO-d_6/Me$_4$Si, 100 MHz): δ 172.56 (1C, CO), 134.30, 133.14, 130.95, 130.30, 130.13, 129.81, 127.54, 127.38, 127.21, 127.13, 127.06, 124.72, 124.62, 124.32, 123.92, 123.62 (16C, ArC), 74.03, 72.84, 71.91, 70.50, 63.80 (5C, COH), 42.71, 38.40, 29.40, 29.31, 26.11, 26.01 (6C, CH$_2$). FTIR (KBr) v_{max} (cm^{-1}): 3410 (NH), 3595-3045 (OH); 3375 (HNSO$_2$); 2925 (CH); 1629 (C=O); 1544 (NH); 1425 (CN); 1311, 1141 (S=O). EA (%) calcd for C$_{28}$H$_{34}$N$_2$O$_8$S·½H$_2$O: C, 59.24; H, 6.21; N, 4.93. Found: C, 59.92; H, 6.09; N, 4.98.

For **P7**: 55% yield; mp 139.9-142.4 ºC. ^{1}H NMR (DMSO-d_6/Me$_4$Si, 300 MHz) δ (ppm): 9.00-9.03 (d, J = 9 Hz, 1H), 8.59-8.61 (d, J = 6 Hz, 1H), 8.20-8.48 (m, 7H), 8.10 (s, 1H), 7.46 (s, 1H), 5.35 (s, 1H), 4.35-4.58 (m, 4H), 3.90-3.97 (m, 2H), 3.38-3.60 (m, 4H), 2.80-2.82 (b, 4H), 0.85-1.24 (m, 10H). ^{13}C NMR (DMSO-d_6/Me$_4$Si, 100 MHz): δ 172.53 (1C, CO), 134.32, 133.17, 130.96, 130.30, 130.13, 129.80, 127.55, 127.39, 127.21, 127.15, 127.06, 124.73, 124.59, 124.32, 123.93, 123.63 (16C, ArC), 74.02, 72.85, 71.91, 70.51, 63.80 (5C, COH), 42.66, 38.47, 29.29, 29.26, 28.48, 26.48, 26.16 (7C, CH$_2$). FTIR (KBr) v_{max} (cm^{-1}): 3419 (NH), 3590-3050 (OH); 3375 (HNSO$_2$); 2929 (CH); 1625 (C=O); 1544 (NH); 1430 (CN); 1308, 1141 (S=O). EA (%) calcd for C$_{29}$H$_{36}$N$_2$O$_8$S·½H$_2$O: C, 59.88; H, 6.41; N, 4.82. Found: C, 59.71; H, 6.27; N, 4.94.

For **P8**: 50% yield; mp 141.1-144.3ºC. ^{1}H NMR (DMSO-d_6/Me$_4$Si, 300 MHz) δ (ppm): 9.00-9.03 (d, J = 9 Hz, 1H), 8.59-8.62 (d, J = 9 Hz, 1H), 8.19-8.48 (m, 7H), 8.05 (s, 1H), 7.45 (s, 1H), 5.32 (s, 1H), 4.32-4.52 (m, 4H), 3.91-3.97 (m, 2H), 3.41-3.59 (m, 4H), 2.82-2.81 (b, 4H), 0.77-1.19 (m, 12H). ^{13}C NMR (DMSO-d_6/Me$_4$Si, 100 MHz): δ 172.55 (1C, CO), 134.33, 133.20, 130.97, 130.31, 130.13, 129.78, 127.54, 127.39, 127.20, 127.17, 127.05, 124.73, 124.57, 124.33, 123.94, 123.63 (16C, ArC), 74.04, 72.86, 71.93, 70.54, 63.82 (5C, COH), 42.60, 38.55, 29.37, 29.16, 28.88, 28.66, 26.51, 26.10 (8C, CH$_2$). FTIR (KBr) v_{max} (cm^{-1}): 3410 (NH), 3525-3050 (OH); 3370 (HNSO$_2$); 2921 (CH); 1637 (C=O); 1540 (NH); 1427 (CN); 1311, 1139 (S=O). EA (%) calcd for C$_{30}$H$_{38}$N$_2$O$_8$S·½H$_2$O: C, 60.49; H, 6.60; N, 4.70. Found: C, 60.47; H, 6.41; N, 4.82.

(e) Further purification of **P4-P8**:

The **P4**-**P8**, obtained using above-mentioned method, are denoted as Series A. Aliquots were purified further as described in detail for **P4**. **P4** (100 mg) was added to 1 mL of methanol and heated in a water bath until the solid dissolved. After cooling to room temperature, a very stable gel formed. The gel was destroyed mechanically with a glass rod, the liquid was removed with a pipette, the solid was washed with cold methanol, and the solid was collected by filtration. This process was repeated 3 times. Finally, the obtained solid was dried under vacuum (~3000 Pa) at 40 ºC for 48 h. The **P4**-**P8** aliquots purified with methanol are designated as Series B. The melting points and the elemental analyses of the **P4**-**P8** of both series are summarized in Table S1.

Table S1. Melting points and elemental analyses (EA) of **Pn** obtained by different protocols.

Pn	Series	Protocol and EA	Melting point (ºC)	C%	H%	N%
P2	A	Washed with water	173.5-175.0	56.75	5.11	5.37
		EA calcd. for $C_{24}H_{26}N_2O_8S\cdot\frac{1}{2}H_2O$		56.35	5.32	5.48
P3	A	Washed with water	167.0-168.5	57.07	5.35	5.31
		EA calcd. for $C_{25}H_{28}N_2O_8S\cdot\frac{1}{2}H_2O$		57.13	5.56	5.33
P4	A	Centrifugation with water and NaCl	131.8-133.5	57.30	5.67	5.30
	B	Gel washed with methanol	132.0-134.0	57.82	5.77	5.19
		EA calcd. for $C_{26}H_{30}N_2O_8S\cdot\frac{1}{2}H_2O$		57.87	5.79	5.19
P6	A	Centrifugation with water and NaCl	127.0-129.5	59.92	6.09	4.98
	B	Gel washed with methanol	128.7-130.5	59.65	6.20	4.95
		EA calcd. for $C_{28}H_{34}N_2O_8S\cdot\frac{1}{2}H_2O$		59.24	6.21	4.93
P7	A	Centrifugation with water and NaCl	139.9-142.4	59.71	6.27	4.94
	B	Gel washed with methanol	140.0-142.5	59.93	6.39	4.85
		EA calcd. for $C_{29}H_{36}N_2O_8S\cdot\frac{1}{2}H_2O$		59.88	6.41	4.82
P8	A	Centrifugation with water and NaCl	141.1-144.3	60.47	6.41	4.82
	B	Gel washed with methanol	142.0-144.5	60.48	6.50	4.73
		EA calcd. for $C_{30}H_{38}N_2O_8S\cdot\frac{1}{2}H_2O$		60.49	6.60	4.70

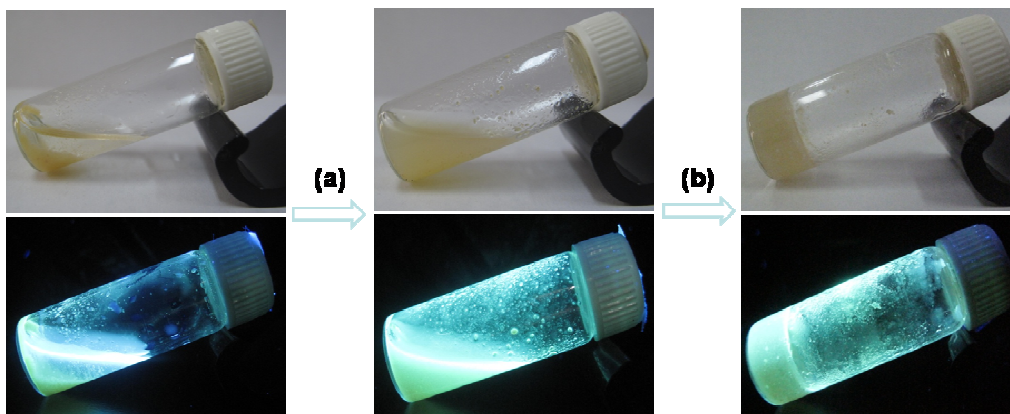**2. Pictures of 2% P7 in 30:70 THF:water mixtures at room temperature**

Figure S1. Pictures of 2% **P7** in 30:70 THF:water mixtures at room temperature. (a) Subjected to vortex mixing at ~1000 rpm for ~30 s. (b) At rest overnight after treatment (a).   Top: under room light. Bottom: under a 365 nm lamp.

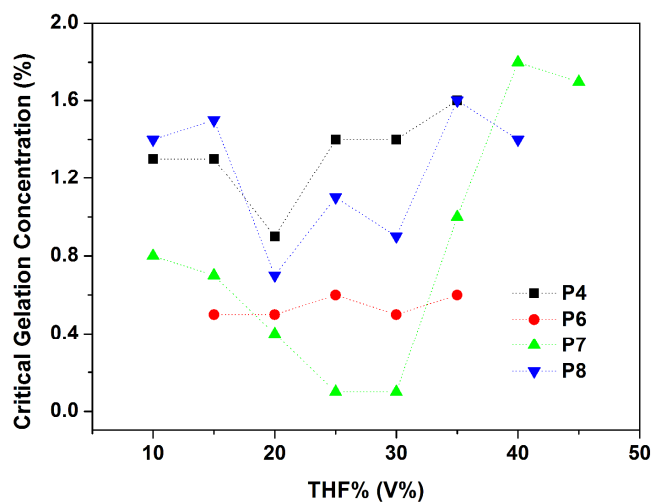**3. Critical gelation concentrations of Pn in liquid mixtures with diffferent THF compositions**

Figure S2. Critical gelator concentrations of **Pn** in liquid mixtures with diffferent THF:water compositions.

4. T_{gel} values of gels in THF:water mixtures as a function of P7 concentration
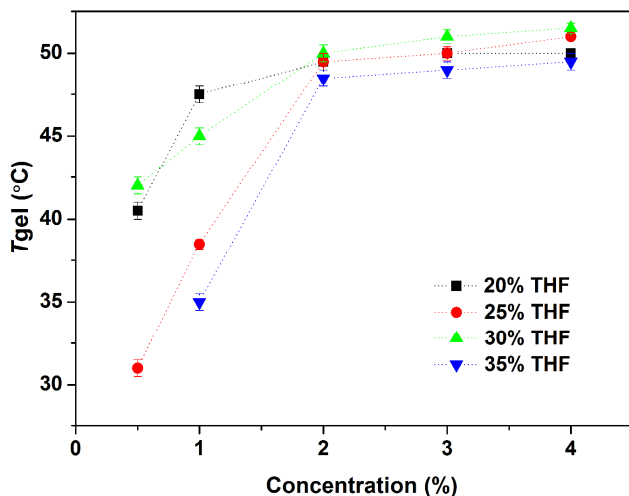
Figure S3. T_{gel} values of gels of **P7** in several THF:water compositions as a function of **P7** concentration. Temperature ranges of vertical bars refer to when the initial and final portions of a gel sample fell on being heated slowly in an inverted tube.

5. T_{gel} values of gels of Pn in THF:water mixtures with different compositions
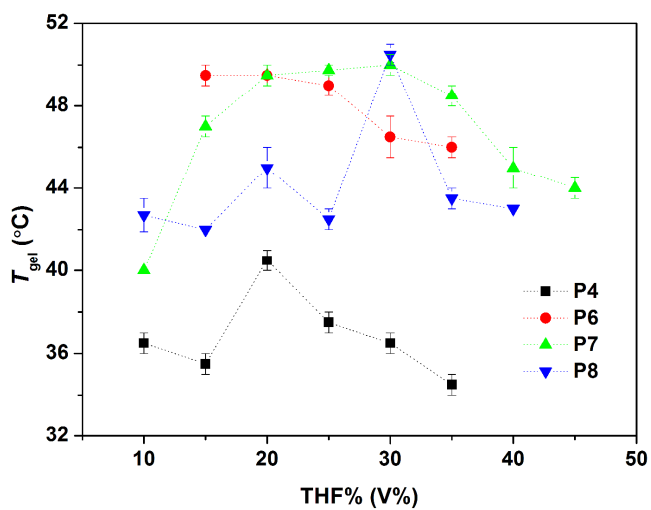
Figure S4. T_{gel} values of gels of 2.0% **Pn** in different THF:water compositions. Temperature ranges of vertical bars refer to when the initial and final portions of a gel sample fell on being heated slowly in an inverted test tube.

6. Molecular structure of Reichardt's dye
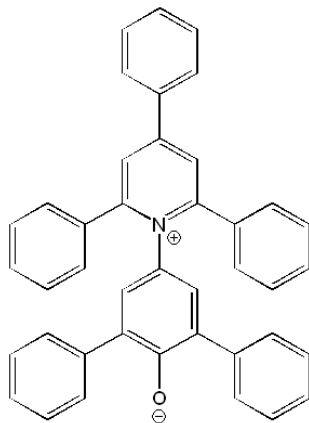
Chart S1. Molecular structure of Reichardt's dye.

7. Table of Hansen solubility parameters for the THF:water mixtures examined and the CGCs of P7

Table S2. Hansen solubility parameters (MPa$^{0.5}$) of different THF:water compositions, their distances (R) in Hansen space from **P7** (δ_p = 8.36 MPa$^{0.5}$, δ_h = 16.89 MPa$^{0.5}$, and δ_d = 16.46 MPa$^{0.5}$), and critical gelator concentrations (%) or appearances of **P7** in various liquids at room temperature.

THF (%)	δ_P	δ_h	δ_d	δ	R	CGC (%) or appearance[a]
100	5.70	8.00	16.80	19.46	9.30	I
95	6.22	9.72	16.74	20.33	7.50	S
90	6.73	11.44	16.67	21.31	5.70	S
80	7.76	14.88	16.54	23.56	2.10	S
70	8.79	18.32	16.41	26.12	1.50	S
60	9.82	21.76	16.28	28.90	5.10	S
50	10.85	25.20	16.15	31.84	8.70	S
45	11.37	26.92	16.09	33.36	10.50	G, 1.7
40	11.88	28.64	16.02	34.90	12.30	G, 1.8
35	12.40	30.36	15.96	36.47	14.10	G, 1.0
33	12.60	31.05	15.93	37.10	14.82	G
30	12.91	32.08	15.89	38.06	15.90	G, 0.1
28	13.12	32.77	15.86	38.70	16.62	G
25	13.43	33.80	15.83	39.66	17.70	G, 0.1
20	13.94	35.52	15.76	41.28	19.50	G, 0.4
15	14.46	37.24	15.70	42.92	21.30	G, 0.7
10	14.97	38.96	15.63	44.57	23.10	G, 0.8
5	15.49	40.68	15.57	46.23	24.90	Sus
0	16.00	42.40	15.50	47.90	26.70	I

[a] [**P7**] = 2.0%, S = soluble, I = insoluble, Sus = suspension.

8. Solubility data for 2.0% P7 in liquid mixtures represented in Hansen space with independent spheres
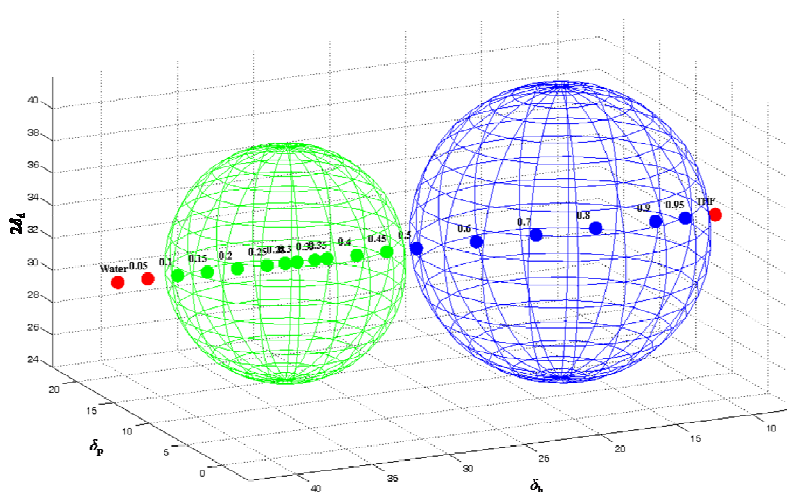

Figure S5. Solubility data for 2.0% **P7** in liquid mixtures represented in Hansen space with independent spheres.   Blue (soluble), green (gel), and red (insoluble).   For the sake of clarity and because very few data points are available, no red spheres are drawn.

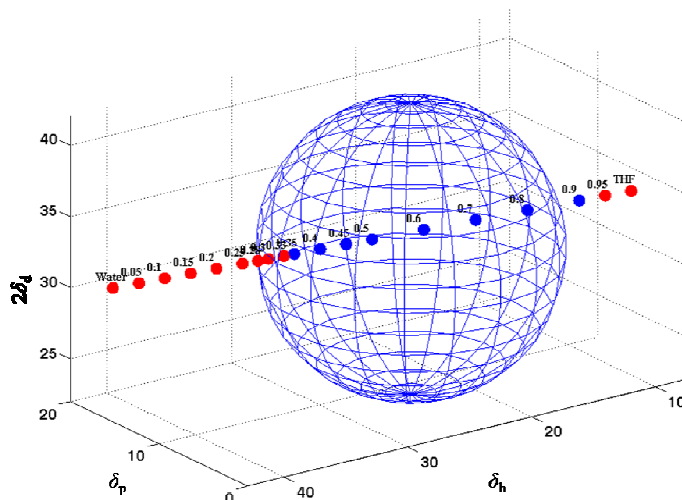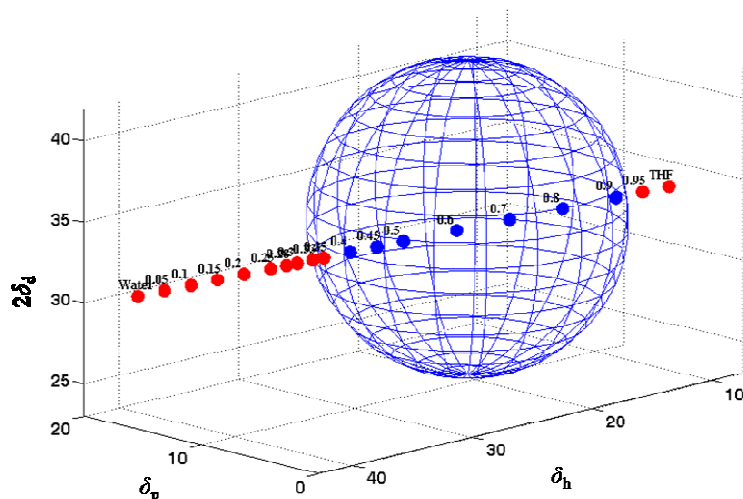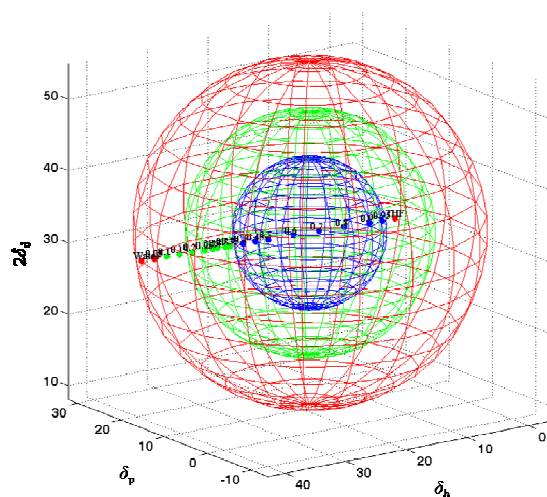**9. Solubility data for 2.0% Pn in liquid mixtures represented in Hansen space with concentric spheres/shells**
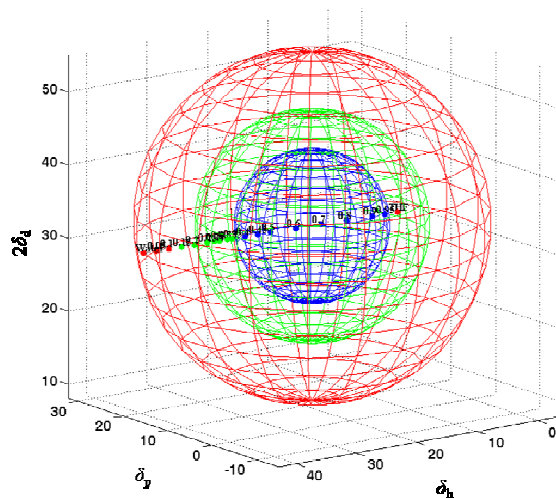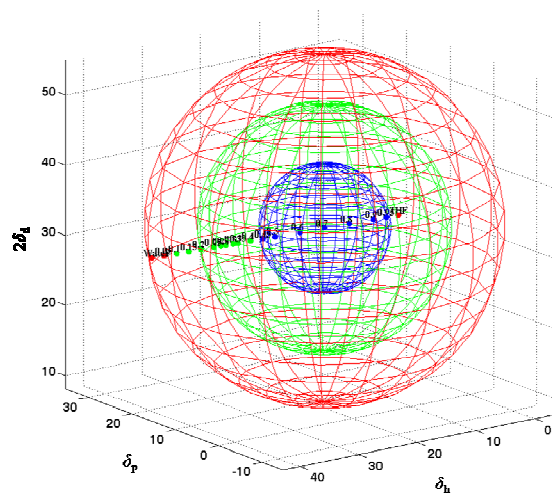

Figure S6. Solubility data for 2.0% **P2** in liquid mixtures represented in Hansen space with spheres.   Blue (soluble), green (gel), and red (insoluble).

Figure S7. Solubility data for 2.0% **P3** in liquid mixtures represented in Hansen space with spheres. Blue (soluble), green (gel), and red (insoluble).

Figure S8. Solubility data for 2.0% **P4** in liquid mixtures represented in Hansen space with spheres. Blue (soluble), green (gel), and red (insoluble).

Figure S9. Solubility data for 2.0% **P6** in liquid mixtures represented in Hansen space with spheres. Blue (soluble), green (gel), and red (insoluble).

Figure S10. Solubility data for 2.0% **P8** in liquid mixtures represented in Hansen space with spheres. Blue (soluble), green (gel), and red (insoluble).

10. Plots of CGCs of Pn as a function of Hansen Solubility Parameters (HSPs)
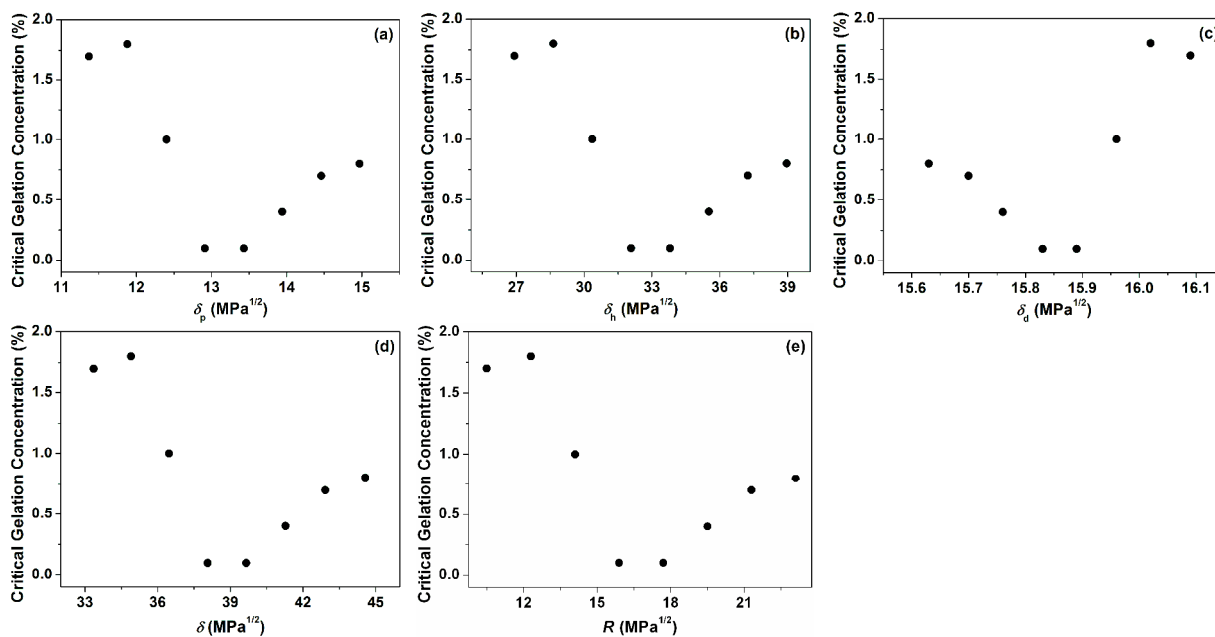

Figure S11. Critical gelation concentrations (CGCs) of **P7** in liquid mixtures gelated as a function of: (a) δ_p, (b) δ_h, (c) δ_d, (d) overall Hansen solubility parameter (δ), and (e) R from **P7** in Hansen space ($\delta_p = 8.36$ MPa$^{0.5}$, $\delta_h = 16.89$ MPa$^{0.5}$, and $\delta_d = 16.46$ MPa$^{0.5}$).
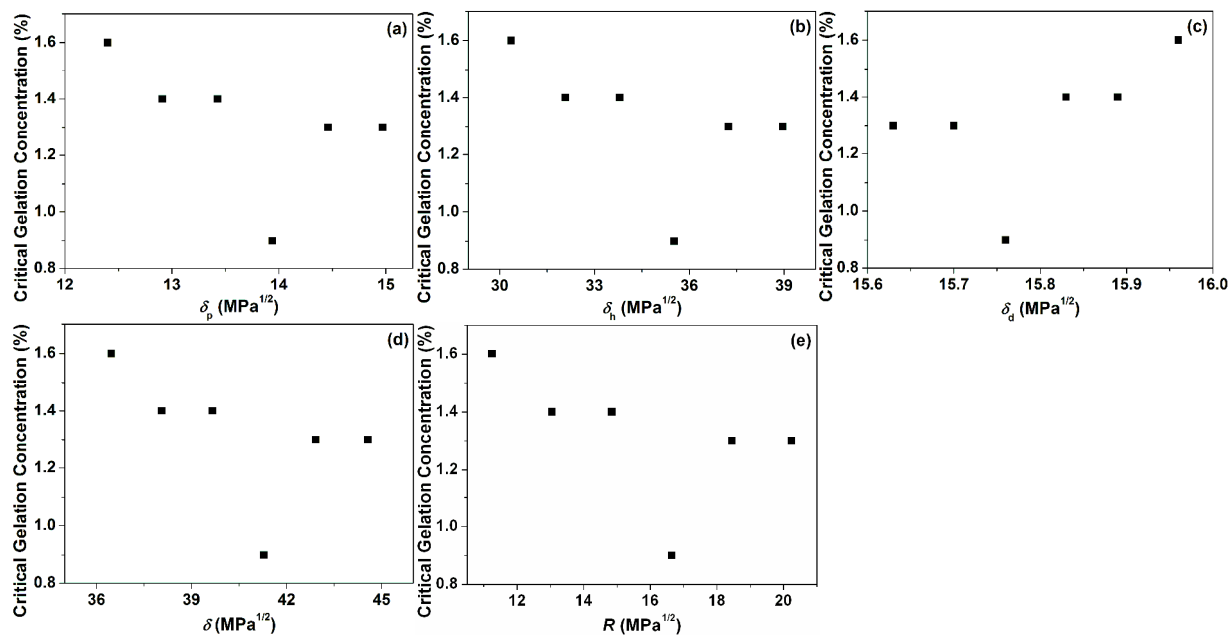
Figure S12. Critical gelation concentrations (CGCs) of **P4** in liquid mixtures gelated as a function of: (a) δ_p, (b) δ_h, (c) δ_d, (d) overall Hansen solubility parameter (δ), and (e) R from **P4** in Hansen space ($\delta_p = 9.18$ MPa$^{0.5}$, $\delta_h = 19.61$ MPa$^{0.5}$, and $\delta_d = 16.36$ MPa$^{0.5}$).
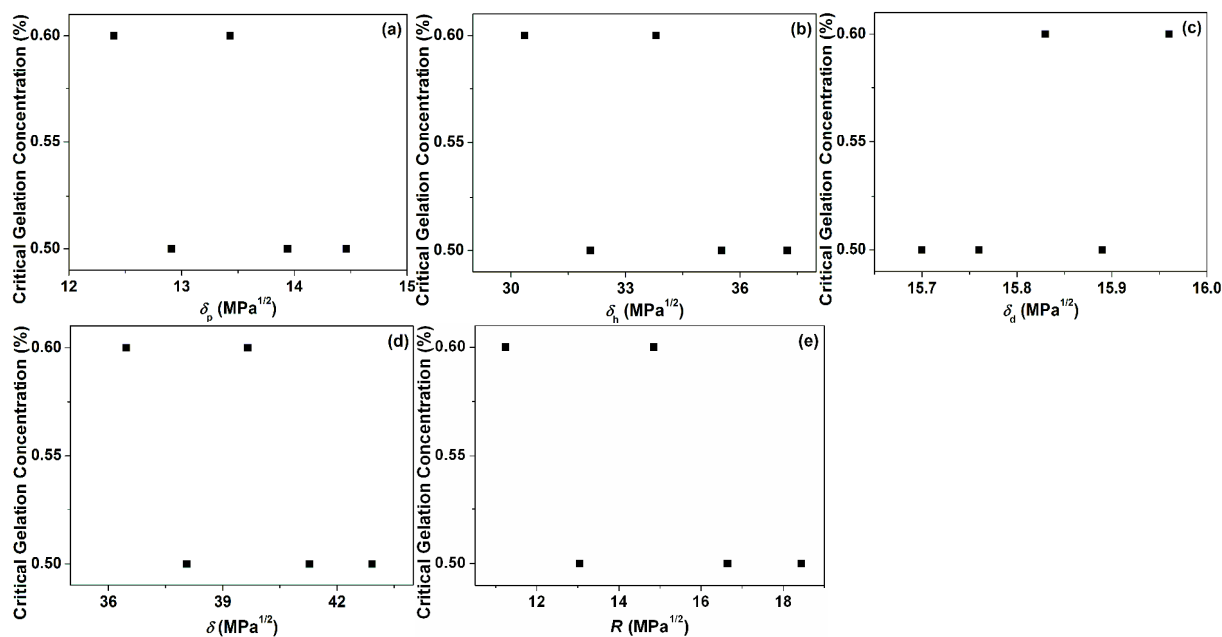

Figure S13. Critical gelation concentrations (CGCs) of **P6** in liquid mixtures gelated as a function of: (a) δ_p, (b) δ_h, (c) δ_d, (d) overall Hansen solubility parameter (δ), and (e) R from **P6** in Hansen space ($\delta_p = 9.18$ MPa$^{0.5}$, $\delta_h = 19.61$ MPa$^{0.5}$, and $\delta_d = 16.36$ MPa$^{0.5}$).
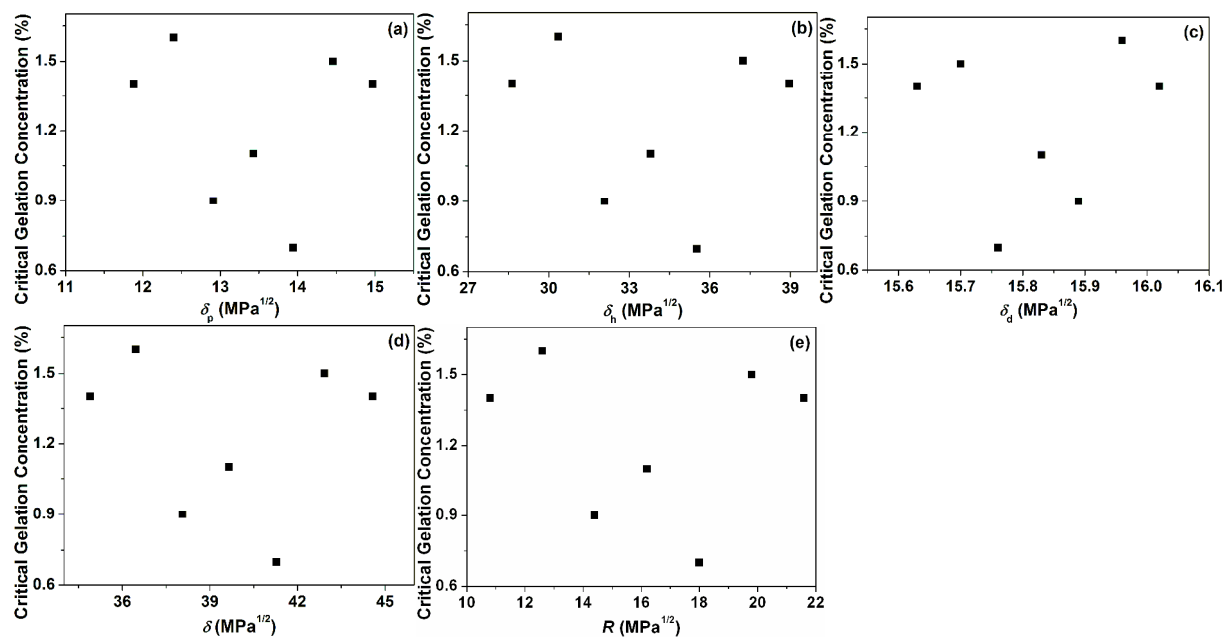
Figure S14. Critical gelation concentrations (CGCs) of **P8** in liquid mixtures gelated as a function of: (a) δ_p, (b) δ_h, (c) δ_d, (d) overall Hansen solubility parameter (δ), and (e) R from **P8** in Hansen space ($\delta_p = 8.79$ MPa$^{0.5}$, $\delta_h = 18.32$ MPa$^{0.5}$, and $\delta_d = 16.41$ MPa$^{0.5}$).

11. POM images of 2% Pn in 20:80 THF:water mixtures
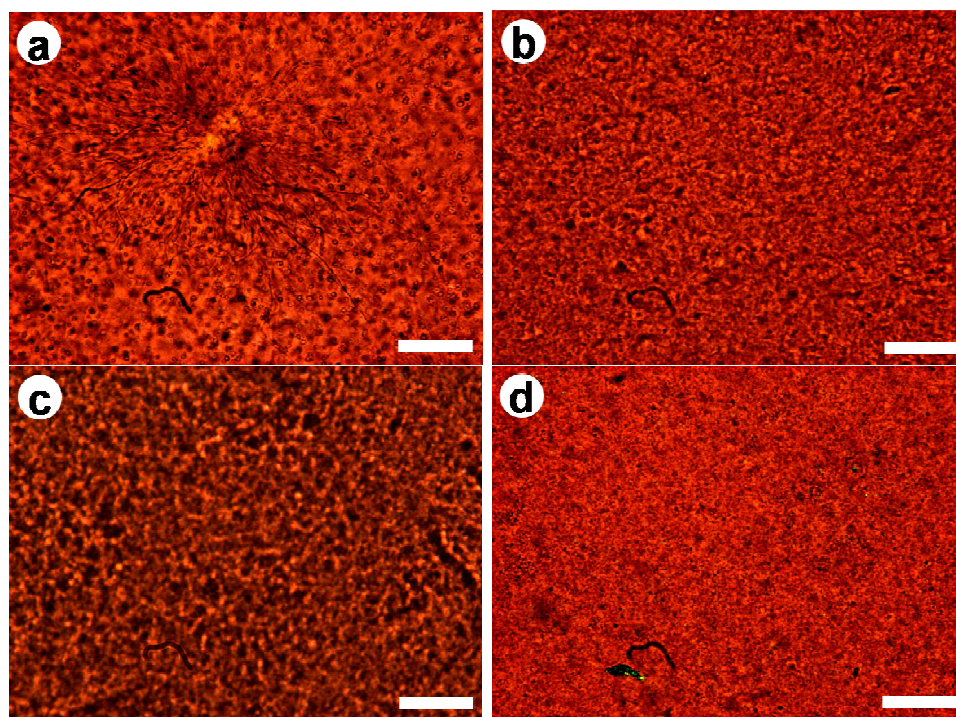

Figure S15. POMs (full-wave plate) of 2.0% **Pn** in 20:80 THF:water liquid mixture: (a) **P4**; (b) **P6**; (c) **P7**; (d) **P8**. (distance bars = 100 μm).

12. SEM images of solids from solutions/sols and of xerogels from gels of 2.0% P7 in THF:water mixtures
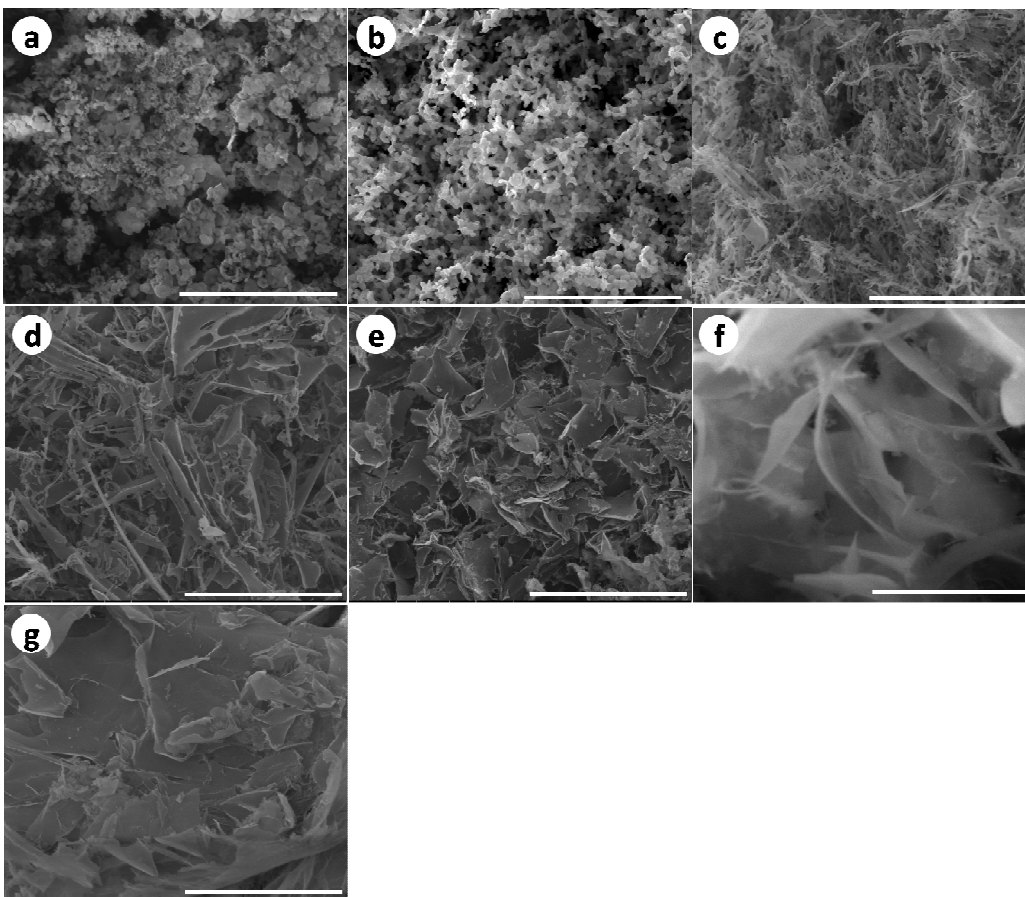

Figure S16. SEM images of solids from solutions/sols of 2.0% **P7** in THF:water mixtures: (a) 95:5, (b) 70:30, and (c) 50:50.   Xerogels from the gels of 2.0% **P7** in THF:water mixtures: (d) 40:60, (e) 30:70, (f) 25:75, and (g) 20:80. (Distance bars = 50 μm).

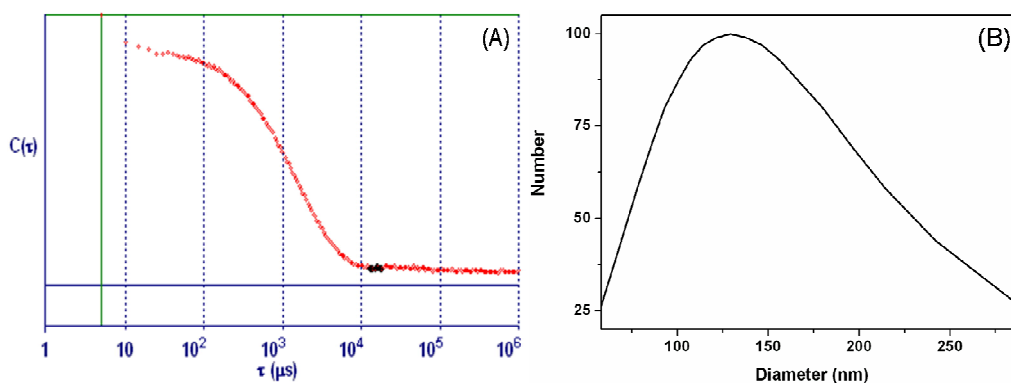## 13. Dynamic light scattering of P7 in THF:water mixtures

Figure S17. (A) Dynamic light scattering correlation function of the scattering particles in the solution/sol of 0.2 % **P7** in 95:5 at 25 ˚C. (B) Distribution of diameters of the particles, with a maximum at ca. 130 nm.

Table S3. The diameters (D, nm) at the maxima in the distributions of the scattering particles in the solutions/sols of 0.2% (3.5×10^{-3} M) **P7** in 95:5, 70:30 and 50:50 THF:water, and of 2% (3.5×10^{-2} M) **P7** in 95:5, 70:30 and 50:50 THF:water at 25 ˚C, and the full widths at half heights (W, nm) of the curves in Figure 5.

[**P7**] (M)		95:5	70:30	50:50
3.5×10^{-3}	D	130	140	530
	W	120	130	460
3.5×10^{-2}	D	1050	1200	1880
	W	140	160	1750

Table S4. Diameters (D, nm) of the scattering particles at the maxima of the distributions in the solutions/sols of 1.1×10^{-5} M **P7** in 95:5, 70:30 and 50:50 THF:water mixtures, and of 1.1×10^{-4} M **P7** in 95:5, 70:30 and 50:50 THF:water mixtures at 25 ˚C, the full widths at half height (W, nm) of their curves.

[**P7**] (M)		95:5	70:30	50:50
1.1×10^{-5}	D	[a]	[a]	500
	W	[a]	[a]	280
1.1×10^{-4}	D	[a]	[a]	520
	W	[a]	[a]	300

[a] No scattering was observed.

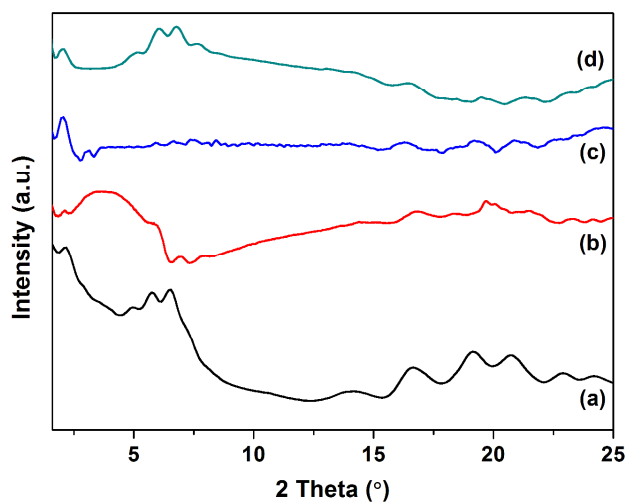## 14. X-ray diffraction patterns of P7

Figure S18. X-ray diffraction patterns of **P7** (Series B): (a) neat powder; (b) a 10% **gel** in 20:80 THF:water, (c) a 7% gel in 30:70 THF:water, and (d) a 10% gel in 40:60 THF:water after subtracting empirically the amorphous scattering of the corresponding liquid mixtures from the total gel diffractograms; see text for details.

Table S5. Comparison of 2θ and d values of the diffraction peaks from neat **P7** and the gels of **P7** in THF:water mixtures.

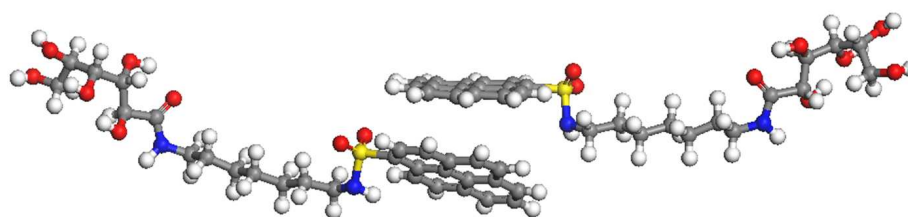| THF:water	[P7] (%)	2θ (°)	Bragg distance d (nm)
(Neat solid)	100	2.12, 4.96, 5.75, 6.55, 14.18, 16.66, 19.13, 20.72	4.16, 1.78, 1.54, 1.35, 0.62, 0.53, 0.46, 0.43
20:80	10	2.12, 3.70, 6.97, 7.98, 14.41, 16.89, 18.48, 19.71, 21.47	4.16, 2.39, 1.27, 1.11, 0.61, 0.48, 0.45, 0.41
30:70	7	2.12, 3.15, 5.99, 6.67, 7.36, 8.43, 14.01, 16.27, 19.2, 20.87	4.16, 2.8, 1.47, 1.3, 1.12, 1.05, 0.63, 0.54, 0.46, 0.43
40:60	10	2.12, 5.2, 6.1, 6.8, 7.69, 16.39, 19.48, 21.28	4.16, 1.7, 1.45, 1.3, 1.15, 0.54, 0.46, 0.42

Figure S19. Proposed packing arrangement and calculated length (4.36 nm, with van der Waals radii of the terminal hydrogen atoms) of an interdigitated **P7** pair.

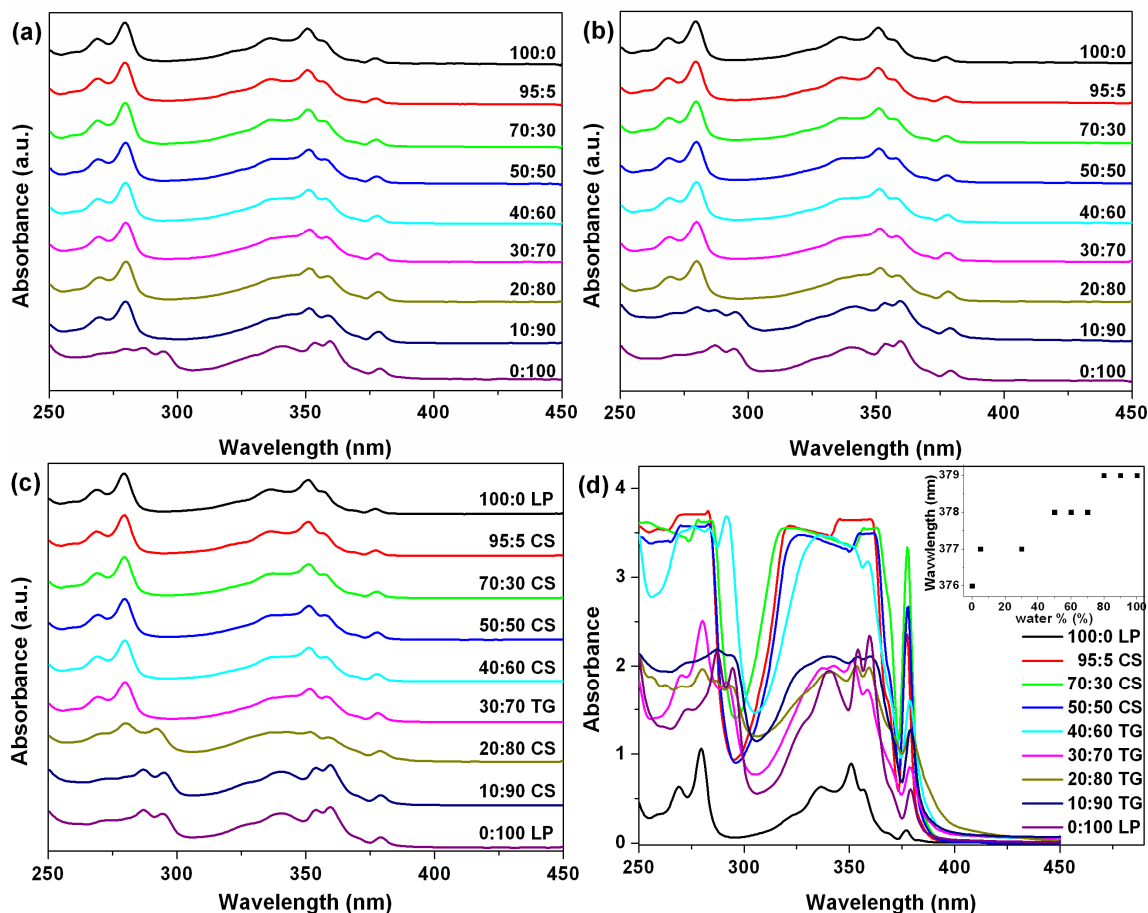## 15. UV-vis spectra of P7 in THF:water mixtures

Figure S20. Vertically offset UV-vis absorption spectra (normalized for intensity at 280 nm) of clear solutions/sols of **P7** in THF:water mixtures at **[P7]** = 1.1×10^{-5} M (a) and 1.1×10^{-4} M (b), and in neat THF (**[P7]** $\sim 2.1 \times 10^{-3}$ M, saturated), neat water (**[P7]** $\sim 3.3 \times 10^{-4}$ M; saturated), and in THF:water mixtures at [**P7**] = 2.6×10^{-3} M (0.15%) (c). UV-vis absorption spectra of solutions/sols in neat THF (**[P7]** $\sim 2.1 \times 10^{-3}$ M, saturated) or in neat water (**[P7]** $\sim 3.3 \times 10^{-4}$ M; saturated), and in different phases of THF:water mixtures (LP = liquid phase, CS = clear solution/sol, TG = transparent gel) at 3.5×10^{-2} M (2%); the inset shows the shift in the wavelength maximum of the absorption band near 376 nm with increasing water content (d). Note that the maximum absorbance range of the spectrophotometer is ca. 3.5; flattened portions of the spectra at this absorbance should be considered only as minimum values.

16. Fluorescence of 2% P7 in THF:water mixtures

Table S6. The values of $I_{379\,nm}/I_{500\,nm}$ and I_1/I_3 of the emission from 2% **P7** in THF:water mixtures.

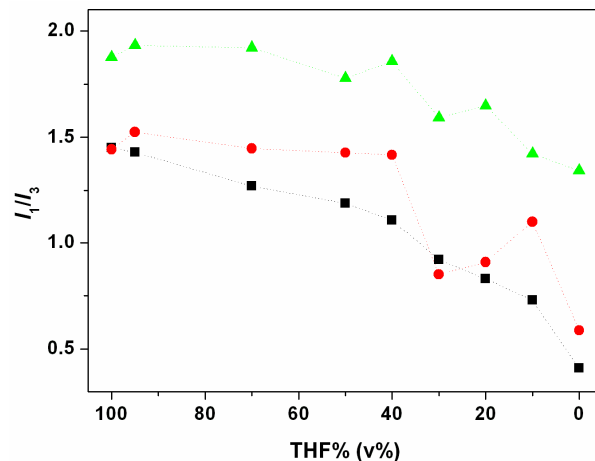| THF:water	100:0	95:5	70:30	50:50	40:60	30:70	20:80	10:90	0:100
$I_{379nm}/I_{500\,nm}$	13.32	1.98	1.12	0.93	0.58	0.46	0.44	0.39	0.08
I_1/I_3	1.45	1.43	1.27	1.19	1.11	0.92	0.83	0.73	0.41

Figure S21. I_1/I_3 values for emission from 2% **P7** in THF:water mixtures, calculated from the emission intensities before and after subtraction of the excimeric contributions at the I_3 wavelengths: (■) before subtraction (from as-obtained spectra), (●) calculated using a deconvolution program (see text), and (▲) calculated by spectral subtraction (see text for details).
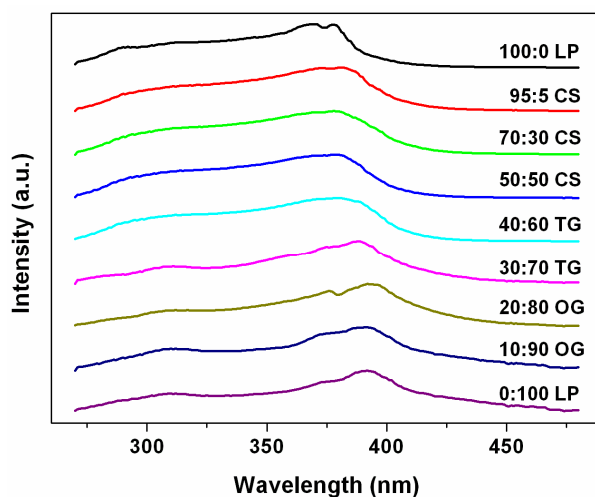

Figure S22. Vertically offset excitation spectra (λ_{em} 500 nm; intensity normalized at 399 nm) of the liquid phases from the mixtures of 2% **P7** in neat THF (dissolved [**P7**] ~2.1 × 10^{-3} M) or in neat water (dissolved [**P7**] ~3.3 × 10^{-4} M), and the spectra of the solutions/sols and the gels of 2% (3.5 × 10^{-2} M, total concentration) **P7** (Series B) in THF:water mixtures at 20 °C. Appearances of the samples: LP = liquid phase, CS = clear solution/sol, TG = transparent gel, OG = opaque gel.

17. Rheology of 2% Pn in THF:water mixtures

Table S7. G', G'', and G'/G'' at strain = 0.01% and yield strain of the gels of 2 % **P7** in THF:water mixtures at 25°C.

THF:water	G' (Pa)	G'' (Pa)	G'/G''	Yield strain (%)
10:90	240 ± 20^a	30 ± 5	7.4 ± 0.1	3.2
20:80	3160 ± 500	340 ± 70	9.3 ± 0.2	14.7
25:75	38500 ± 3900	3780 ± 410	10.2 ± 0.1	31.6
28:72	47500 ± 8970	4310 ± 790	11.0 ± 0.2	60.1 ± 5
29:71	52700 ± 7980	4580 ± 690	11.5 ± 0.15	150 ± 5.5
30:70	47100 ± 9460	3870 ± 780	12.2 ± 0.2	200 ± 6
31:69	48600 ± 4900	4330 ± 450	11.2 ± 0.1	160 ± 4
33:67	50000 ± 5060	4640 ± 450	10.8 ± 0.1	147 ± 7
35:65	67400 ± 5390	6290 ± 500	10.7 ± 0.08	147
40:60	65400 ± 6550	6200 ± 620	10.5 ± 0.1	56.3
45:55	37900 ± 1880	3660 ± 180	10.3 ± 0.05	46.4

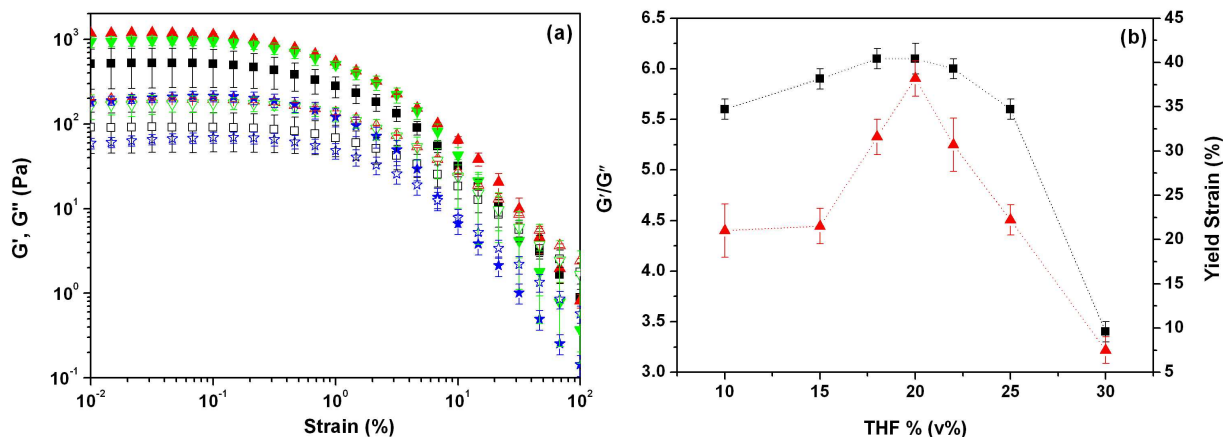^{a} Deviations are based on averages of 3 runs with different aliquots.

Figure S23. (a) Log-log strain sweep (frequency = 1.0 Hz) for gels of 2.0% **P4** in $v{:}v$ (■) 10:90, (▲) 20:80, (▼) 25:75, and (★) 30:70 THF:water mixtures at 25°C. G', closed symbols, and G'', open symbols. (b) Plot of the values of G'/G'' (■) at strain = 0.01% and yield strain (▲) versus volume % of THF in the gels of 2.0% **P4** in THF:water mixtures at 25°C. Data are obtained from three trials, and vertical bars are one standard deviation.

Table S8. The value of G', G'', G'/G'' at strain = 0.01% and yield strain of the gels of 2.0% **P4** in THF:water mixtures at 25°C.

THF:water	G' (Pa)	G'' (Pa)	G'/G''	Yield strain (%)
10:90	770 ± 80^a	140 ± 15	5.6 ± 0.1	21 ± 3
15:85	1090 ± 100	190 ± 20	5.9 ± 0.1	21.5 ± 2
18:82	1270 ± 130	210 ± 20	6.1 ± 0.1	31.6 ± 2
20:80	1180 ± 180	190 ± 30	6.1 ± 0.15	38.2 ± 2
22:78	1420 ± 150	230 ± 20	6.0 ± 0.1	30.7 ± 3
25:75	920 ± 90	170 ± 20	5.6 ± 0.1	22.2 ± 1.7
30:70	210 ± 20	60 ± 5	3.4 ± 0.1	7.5 ± 1.5

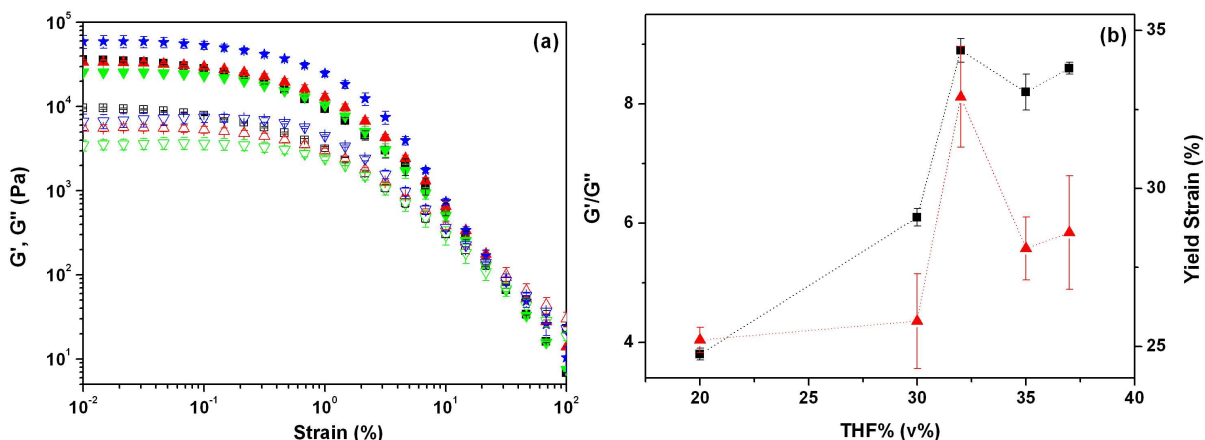[a] Deviations are based on averages of 3 runs with different aliquots.

Figure S24. (a) Log-log strain sweep (frequency = 1.0 Hz) for gels of 2.0% **P6** in v:v (■) 20:80, (▲) 30:70, (▼) 35:65, and (★) 37:63 THF:water mixtures at 25°C. G', closed symbols, and G'', open symbols. (b) Plot of the values of G'/G'' (■) at strain = 0.01% and yield strain (▲) versus volume % of THF in the gels of 2.0% **P6** in THF:water mixtures at 25°C. Data are obtained from three trials, and vertical bars are one standard deviation.

Table S9. The value of G', G'', G'/G'' at strain = 0.01% and yield strain of the gels of 2% **P6** in THF:water mixtures at 25°C.

THF:water	G' (Pa)	G'' (Pa)	G'/G''	Yield strain (%)
20:80	36000 ± 3600	9570 ± 960	3.8 ± 0.1	25.2 ± 0.4
30:70	33800 ± 5070	5540 ± 820	6.1 ± 0.15	25.8 ± 1.5
32:68	61000 ± 12250	6860 ± 1370	8.9 ± 0.2	32.9 ± 1.6
35:65	26000 ± 7880	3170 ± 950	8.2 ± 0.3	28.1 ± 1
37:63	58900 ± 5890	6850 ± 690	8.6 ± 0.1	28.6 ± 1.8

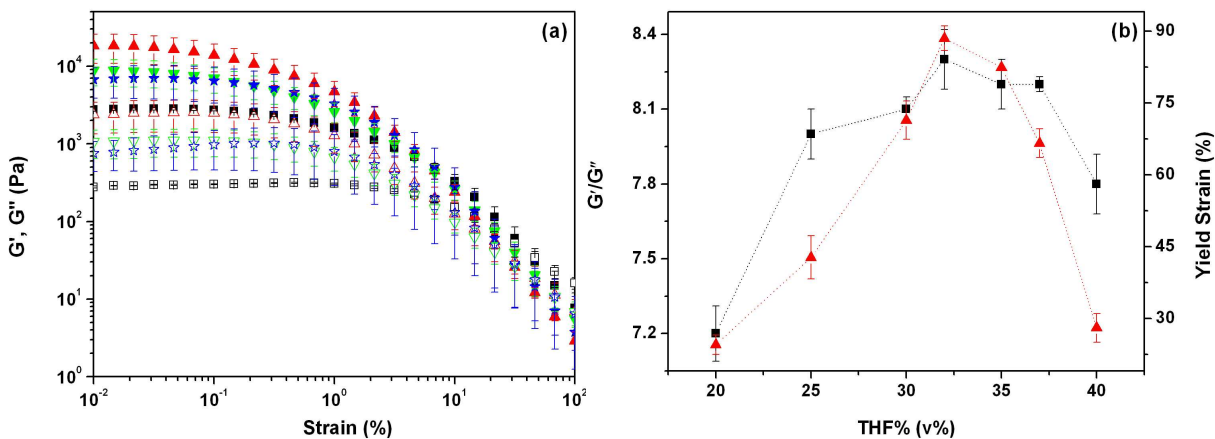[a] Deviations are based on averages of 3 runs with different aliquots.

Figure S25. (a) Log-log strain sweep (frequency = 1.0 Hz) for gels of 2.0 % **P8** in *v:v* (■) 20:80, (▲) 25:75, (▼) 30:70, and (★) 40:60 THF:water mixtures at 25°C. *G′*, closed symbols, and *G″*, open symbols. (b) Plot of the values of *G′/G″* (■) at strain = 0.01% and yield strain (▲) versus volume % of THF in the gels of 2 % **P8** in THF:water mixtures at 25°C. Data are obtained from three trials, and vertical bars are one standard deviation.

Table S10. The value of *G′, G″, G′/G″* at strain = 0.01% and yield strain of the gels of 2% **P8** in THF:water at 25°C.

THF:water	*G′* (Pa)	*G″* (Pa)	*G′/G″*	Yield strain (%)
20:80	2750 ± 300 [a]	380 ± 40	7.2 ± 0.11	24.5 ± 2
25:75	10900 ± 1090	1350 ± 140	8 ± 0.1	42.7 ± 4.5
30:70	8870 ± 440	1070 ± 50	8.1 ± 0.05	71.4 ± 4
33:67	7030 ± 840	850 ± 100	8.3 ± 0.12	88.5 ± 2.6
35:65	6710 ± 670	820 ± 70	8.2 ± 0.1	82.4
37:63	9770 ± 490	1190 ± 60	8.2 ± 0.05	66.6 ± 3
40:60	3080 ± 370	390 ± 50	7.8 ± 0.12	28 ± 3

[a] Deviations are based on averages of 3 runs with different aliquots.
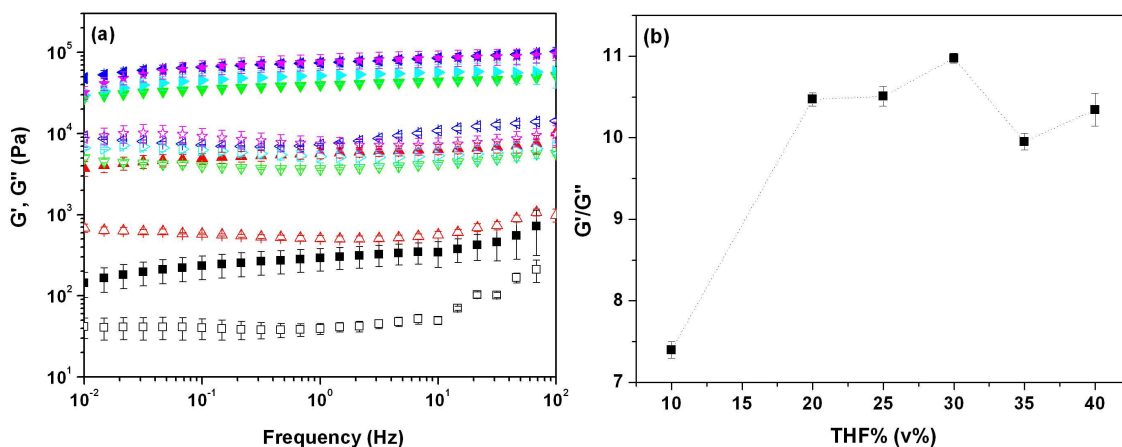

Figure S26. (a) Log-log frequency sweeps (strain = 0.1%) for gels of 2.0 % **P7** in (■) 10:90, (▲) 20:80, (▼) 25:75, (◀) 30:70, (▶) 35:65 and (★) 40:60 THF:water mixtures at 25°C. *G′*, closed symbols, and *G″*, open symbols. (b) Plot of the values of *G′/G″* (■) at frequency = 1 Hz versus volume % of THF in the frequency sweeps. Data are obtained from three trials, and vertical bars are one standard deviation.

18. Gel rheology and Hansen solubility parameters

Table S11. Hansen solubility parameters (MPa$^{0.5}$) of liquid mixtures with different THF volume compositions, and the values of G'/G'' at strain = 0.01% of the gels of 2.0% **P7** in THF:water mixtures at 25°C.

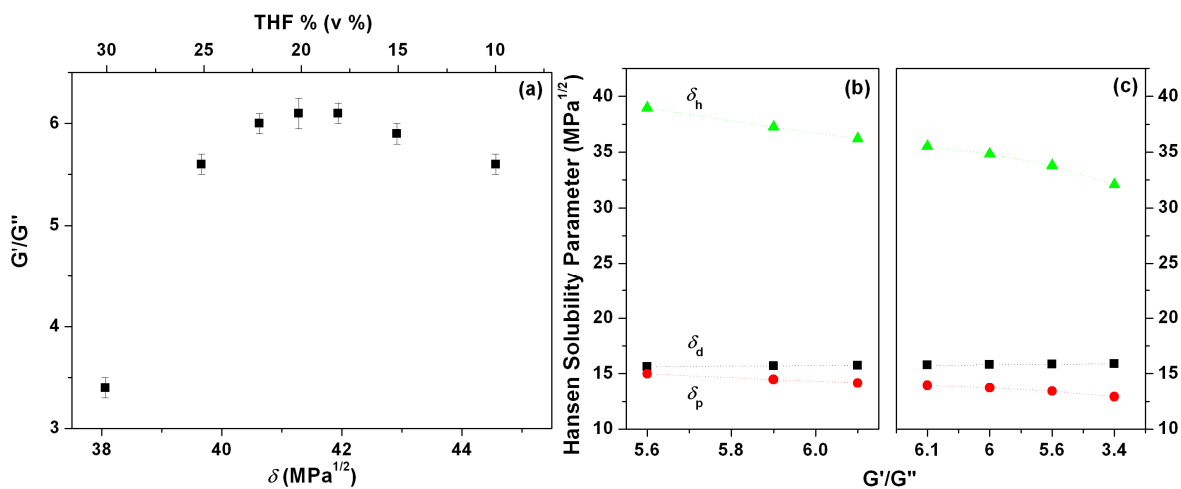| THF (%)	δ_p	δ_h	δ_d	δ	G'/G''
45	11.37	26.92	16.09	33.36	10.3 ± 0.05
40	11.88	28.64	16.02	34.90	10.5 ± 0.1
35	12.40	30.36	15.96	36.47	10.7 ± 0.08
33	12.60	31.05	15.93	37.10	10.8 ± 0.1
31	12.81	31.74	15.90	37.74	11.2 ± 0.1
30	12.91	32.08	15.89	38.06	12.2 ± 0.2
29	13.01	32.42	15.88	38.38	11.5 ± 0.15
28	13.12	32.77	15.86	38.70	11.0 ± 0.2
25	13.43	33.80	15.83	39.66	10.2 ± 0.1
20	13.94	35.52	15.76	41.28	9.3 ± 0.2
10	14.97	38.96	15.63	44.57	7.4 ± 0.1

Figure S27. Effect of overall Hansen solubility parameter (δ) and the volume fraction of THF (a), and the individual Hansen solubility parameter (b and c) on the value of G'/G'' at strain = 0.01% of the gels of 2.0% **P4** in THF:water mixtures.
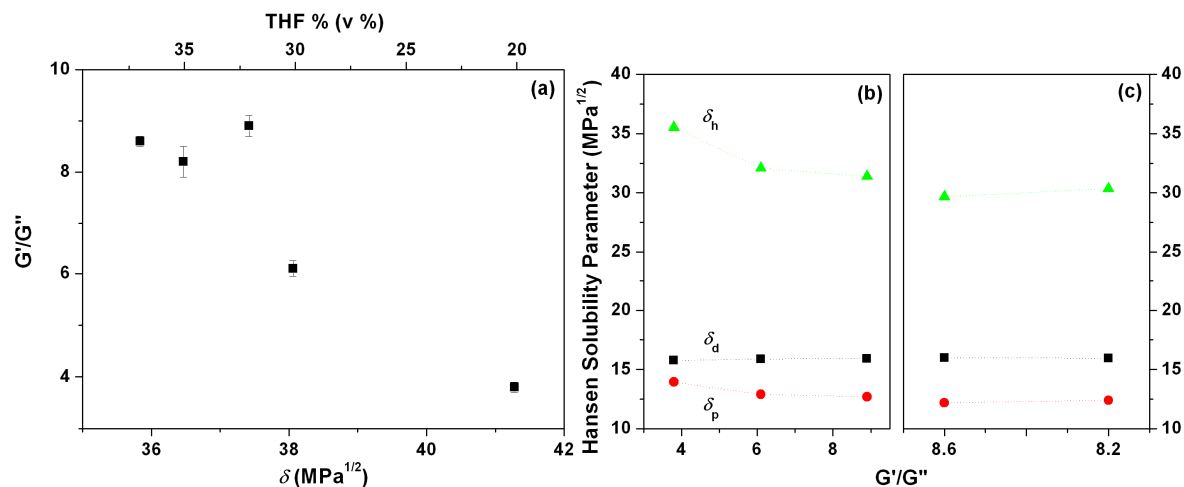
Figure S28. Effect of overall Hansen solubility parameter (δ) and the volume fraction of THF (a), and the individual Hansen solubility parameter (b and c) on the value of G'/G'' at strain = 0.01% of the gels of 2.0% **P6** in THF:water mixtures.
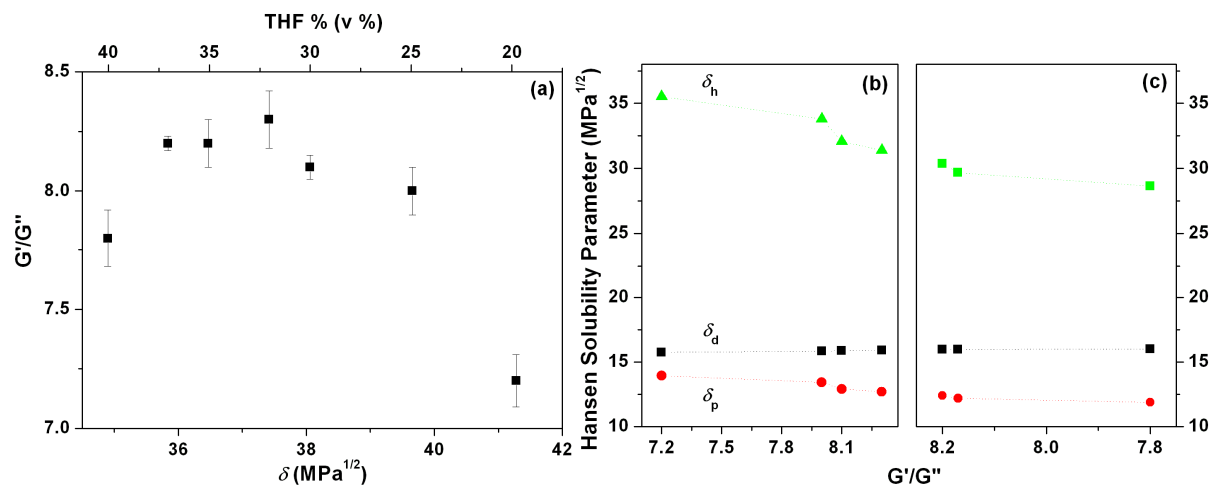

Figure S29. Effect of overall Hansen solubility parameter (δ) and the volume fraction of THF (a), and the individual Hansen solubility parameter (b and c) on the value of G'/G'' at strain = 0.01% of the gels of 2.0% **P8** in THF:water mixtures.

References

(1) Ezzell, S. A.; McCormick, C. L. *Macromolecules* **1992**, *25*, 1881-1886.

(2) Yan, N.; Xu, Z.; Diehn, K. K.; Raghavan, S. R.; Fang, Y.; Weiss, R. G. *Langmuir* **2013**, *29*, 793-805.

(3) Yan, N.; He, G.; Zhang, H.; Ding, L.; Fang, Y. *Langmuir* **2010**, *26*, 5909-5917.